Response 1

Introduction

We thank referee #1 for a close reading of this manuscript and suggestions for improvement. In the following, we explain how we have addressed the reviewer's comments (comments in blue, responses in black). We refer to actual changes in the text using the original page/line numbers in the downloadable pdf-file on the interactive discussion webpage. We summarize additional information from several new figures added to the supplement: one set of figures showing >51 µm POC:^{234}Th, PIC:^{234}Th and BSi:^{234}Th profiles at all stations (Fig. S1), and three figures synthesizing phytoplankton cell count data from co-author Barney Balch (Figs., 2, 3 and 4). The changes in main text and supplement are appended after these responses.

Comment 1. The authors fit the classic power-law curve of Martin et al. to their flux profiles. As they point out, this requires some careful thought about the relevant export depth. To avoid this, and to make comparison between stations simpler, an alternative is the exponen- tial fit of Buesseler and Boyd (2009, L&O). If one makes the assumption that sinking speed is constant with depth, the estimate of remineralisation length scale is indepen- dent of choice of export depth (see e.g. Marsay et al., 2015, PNAS). Of course, the authors would have to check whether the exponential fit was robust for their data. In the discussion (page 2869), the authors actually switch to a discussion of remineralisation length scale which is inconsistent with the use of transfer efficiency and 'b' up to that point. Perhaps reframing the manuscript in terms of remineralisation length scale would be useful?

In Section 4.7, we use the term "remineralization length-scale" to conceptually differentiate POC transfer from BSi-rich (page 2868, lines 18-19) and PIC-rich stations (page 2869, line 20) across GB1 and GB2. We agree with the reviewer that this conceptual use of the term can be erroneously associated with an exponential [POC] profile fit, which we do not apply to the POC flux or >51 µm POC concentration profiles

in this manuscript. Therefore, we have removed this term from those two particular parts of Section 4.7.

We have decided to continue using power law-derived attenuation coefficients and transfer efficiency (T_{100}, or the ratio of POC flux 100 m below z_{PAR} to POC flux at z_{PAR}) to describe POC transfer in the mesopelagic zone throughout Section 4. Because we measured >51 μm [POC] up to 1000 m in depth, a power-law fit would be superior to a single exponential fit, while an exponential fit would work best above ~300 m (Lam and Bishop, 2007, Deep Sea Research II; Buesseler and Boyd, 2009, Limnology and Oceanography). Moreover, fitting >51 μm [POC] profiles to a power law is conceptually significant because it assumes that, at steady-state, [POC] at a given depth is only governed by the sinking flux and loss due to remineralization and particle disaggregation, and that these loss rates are depth-dependent (Lam and Bishop, 2007, Deep Sea Research Part II). Similarly, we focus on T_{100}, as defined in Buesseler and Boyd (2009), to describe POC flux changes from a consistently defined export depth in the most dynamic depth range below the euphotic zone.

Comment 2. The paper provides some interesting particle composition data, which are used to explain trends in POC flux and suggest a strong role of ecosystem structure. It would be beneficial to the interpretation to include more information on the phytoplankton com- munity composition in the study regions (using past studies if in situ data concurrent with sampling are not available). This would provide further weight to the explanations hypothesised by the authors. A plot showing diatom vs coccolithophore dominated regions based on PIC and BSi ratios could be a useful addition.

We agree with reviewer #1 that more information on the phytoplankton community at all stations across GB1 and GB2 would strengthen our hypotheses connecting ecosystem composition to POC transfer, which are currently based on >51 μm BSi and PIC concentrations. To address this, we compared our [BSi] and [PIC] measurements to coccolithophore and diatom cell counts measured by co-author Barney Balch at corresponding stations and have added 3 supplementary figures (Figs. S2, S3, S4). The comparisons show that total coccolithophores and diatoms in the euphotic zone are

significantly and positively correlated with >51 µm [PIC] and [BSi] at z_{PAR}, respectively ($p<0.05$). This supports our use of biomineral concentrations to infer phytoplankton community structure across the Great Calcite Belt. The caveats of this comparison and methodology involved in the phytoplankton cell counts are discussed in the supplement.

We now refer to these supplementary figures in the main text, Section 4.7 (pages 2867, 2868), where we discuss ecosystem composition in terms of >51 µm [BSi] and [PIC] measurements, and in the Fig. 10 caption. Notably, Fig. S4 demonstrates that several stations which we have interpreted to be "diatom-dominated" because >51 µm [PIC]:[BSi]<1 (e.g., page 2868, lines 9-11) exhibit more coccolithophore than diatom cell counts in the euphotic zone. Even though this may be due to the different size fractions that are being compared, this observation has persuaded us to reword our descriptions of stations as "dominated" by coccolithophores (if [PIC]:[BSi]>1) or diatoms (if [PIC]:[BSi]<1) in Section 4.7. Instead, we describe such stations as either exhibiting higher "relative abundances" of coccolithophores (if [PIC]:[BSi]>1) or diatoms (if [PIC]:[BSi]<1) in the euphotic zone.

Comment 3. The authors have collected a wealth of data on particle composition with depth. It would be beneficial to show profiles of ratios of Th with POC, PIC, and BSi to give an idea of the variability with depth and hence how appropriate the choice of the ratio at a depth of ZPAR is for calculating the export flux. This information could perhaps be included in supplementary information.

We have added a four-part supplementary Fig. S1, which shows profiles of all >51 µm POC: ^{234}Th, PIC: ^{234}Th and BSi: ^{234}Th measurements at each station. The panels also indicate depths corresponding to z_{PAR}, $z_{Th/U}$ and, for POC:^{234}Th, 100 m below z_{PAR}. Note that the PIC: ^{234}Th and BSi: ^{234}Th profiles do not extend far below the euphotic zone because there are fewer >51 µm [PIC] and [BSi] measurements at such depths. We have modified section 2.3 to reflect this. Moreover, although the PIC: ^{234}Th and BSi: ^{234}Th panels do not show interpolated values at $z_{Th/U}$, the measurements available should give readers a sense of how variable these metrics are at depths close to $z_{Th/U}$, and how choosing $z_{Th/U}$ as an export depth would hypothetically influence the PIC: ^{234}Th and BSi:

^{234}Th values used in biomineral export flux calculations. We add a reference to Fig. S1 in Sect. 3 (page 2856, line 22) and Sect. 4.4 (page 2862, line 21).

Comment 4. Page 2845, line 3: replace "~1000 m" with "(from the base of the euphotic zone to ~1000 m)"

Changed on page 2845, line 3.

Comment 5. Page 2845, line 8: add reference (maybe Kwon et al. 2009 Nature)

We added this reference on page 2845, line 8.

Comment 6. Page 2845, line 25: replace "remaining intact on its way down", with "reaching the deep ocean"

Changed on page 2845, line 25.

Comment 7. Page 2848, line 21: give duration of pumping and volume of water pumped

We included this information in an additional sentence on page on 2848, line 28.

Comment 8. Page 2849, line 27: give duration of acid fuming

Added detail on page 2849, line 27.

Comment 9. Page 2850, line 11-13: 'We focus our assumption. ….because we assume they contribute disproportionally to sinking fluxes'. Are the authors able to test this assumption with their dataset? The <51um data which were collected do not seem to be used in the manuscript?

We are not able to test this assumption with the data available, as we would need measurements of the size distribution of actual sinking particles collected by sediment traps, but no sediment traps were deployed on these cruises. The <51 μm [POC] measurements are used in calculating the fraction of [POC] that is in the >51 μm size-

fraction. We use this metric in the discussion to discuss the association between >51 µm [BSi] at $_{zPAR}$, the >51 µm [POC] attenuation coefficient and particle size distribution (Sect. 4.7, Fig. 10).

Comment 10. Page 2853, line 4: Why is the 0.3% light level chosen to represent euphotic depth, when it is more commonly defined as 1%?

The Niskin bottles were tripped at depths corresponding to light levels in incubation experiments being conducted on board (Balch et al., in prep). The screening used for the incubation experiments was approximately 0.3% surface PAR, and so this is the light level at which the Niskins were tripped. We have added a line to section 2.1 (page 2848, line 8) to explain this. Because most export flux studies use export depths corresponding to light levels between 0.1% and 1% PAR (e.g., Jerlov, 1968; Poulton et al., 2006, Global Biogeochemical Cycles; Buesseler and Boyd, 2009, Limnology and Oceanography), we found it appropriate to choose depths at 0.3% PAR in order to keep our data set consistent with other depth-specific measurements from the Niskin casts.

Comment 11. Page 2854, line 4-6: The authors should identify somewhere (one of the tables?) which stations did not show a classic Martin curve.

In Table 2, we indicate which stations did not exhibit a significant Martin curve for >51 µm [POC] by writing "no fit" into the corresponding row of column four (titled, ">51 µm [POC] attenuation"). As we do not use Martin curve fits of <51 µm [POC] profiles in this manuscript, we do not report the attenuation coefficients or significance of these fits in Table 2.

Comment 12. Page 2858: The authors use 'productivity' or 'primary productivity' when they mean (satellite-derived) 'chlorophyll'.

On page 2858, we have replaced "productivity" with "chlorophyll".

Comment 13. Page 2859, line 23-27: could be worth tabulating these data from other studies to allow reader to easily compare

We decided not to tabulate these ^{234}Th and POC flux measurements, originally compiled in Le Moigne et al. (2013, Earth System Science Data), because the table would have over two-hundred entries. We added a clarification on line 23 of page 2859 that all the data from other the citations on lines 23-27 are included in this compilation. Instead of tabulating these data, we decide to report the mean and standard deviation of all the compiled fluxes alongside the mean and standard deviation of the fluxes from GB1 and GB2 on lines 22-28.

Comment 14. Page 2861, lines 14-16: Maiti et al. actually showed a strong correspondence between PP and export (just the direction of the relationship was opposite to previous studies).

We corrected an error in the reference here on page 2861 line 16, which should read "Maiti et al., 2012" rather than "Maiti et al., 2010." Maiti et al. (2012, Deep Sea Research Part II) report ^{234}Th-derived POC export fluxes from a highly productive eddy in the Central Pacific through the decline of a diatom bloom, as well as from a site west of the eddy influence. Contrary to the hypothesis that such high-productivity eddies export proportional amounts of carbon, they found that there was no correlation between primary productivity and POC export in the eddy, and no difference in export efficiency between the eddy site and non-eddy site. For this reason, we find it appropriate to cite Maiti et al. (2012) here when commenting on the lack of correlation between primary productivity and POC export in our dataset.

Comment 15. Page 2862, discussion of T100>1 values: if the sampling took place post-bloom, when PP is declining but export is still high, this may result in ratios >1, i.e. non steady state (Henson et al. 2015, GBC).

We acknowledge that sampling after a bloom/during bloom decline could decouple phytoplankton and zooplankton-driven particle export (Henson et al., 2015, Global Biogeochemical Cycles), generating higher POC fluxes below the export depth and causing $T_{100}>1$. However, there is no evidence from the satellite chlorophyll imagery that sampling for those five particular stations with $T_{100}>1$ took place during a bloom decline. We have added a sentence to page 2862, line 8 to reflect this.

Comment 16. Page 2862, line 25: Are the authors able to specify the "sampling issue"?

We do not have an explanation for why the POC:^{234}Th at GB1-25 increases, but note that this station had the lowest attenuation of POC (Table 2) and is the only station where POC: ^{234}Th consistently increases with depth in the upper 400 m. Poor particle distributions on prefilters around the depth of z_{PAR} at GB2-106 may explain the increasing POC: ^{234}Th below z_{PAR} (Fig S1b). We have added a sentence to page 2862, line 25 that reflect this.

Comment 17. Page 2864, line 20-24: sentence could be made clearer, also repeated "2.199"?

We clarified the wording on lines 20-24 of page 2864, and deleted the extra "2.199".

Comment 18. Page 2867, line 1: "further strengthening"…. Do the fits of any of the other stations improve if only looking at upper 500 m? If attenuation over only upper 500 m was plotted against [BSi] and [POC], is a higher correlation observed?

There are only eight stations with >51 µm [POC] profiles that fit significantly ($p<0.05$) to a Martin curve between z_{PAR} and 500 m, including GB1-85, compared with 21 stations that do significantly fit to a Martin curve between z_{PAR} and 800-1000 m. For these 8 stations, the correlation between these upper 500 m b-values and >51 µm [BSi] at z_{PAR} is stronger ($r^2=0.53$ compared to $r^2=0.35$ in Fig. 10a). However, this correlation is weaker than when only the 500 m b-value at GB1-85 is included in the regression and all the other 20 b-values are from fits to deep >51 µm [POC] (r2=0.60) (dashed line in Fig. 10a). Thus, we do not find this 8-point regression to strengthen the association between >51 µm [BSi] and POC transfer in the mesopelagic zone.

There is no correlation between these eight upper 500 m b-values and % >51 µm [POC] at z_{PAR}.

Comment 19. Page 2868, line 22: what is the 'model diatom community'?

On line 22, the "model diatom community" refers to diatom-dominated communities that efficiently export large, BSi- and POC-rich aggregates out of the euphotic zone, as we describe on page 2867, lines 7-10 (Michaels and Silver, 1998, Deep Sea Research; Buesseler 1998, Global Biogeochemical Cycles; Thomalla et al., 2006, Deep Sea Research Part II). We discuss GB1-85 as a model diatom community in the previous paragraph on page 2868, starting at line 8. We decided to add some text to clarify this on line 22 of page 2868.

Comment 20. Page 2879, line 1-5: Figure 10b does not show a clear separation of diatom versus coccolithophore-dominated regions. Is there any statistical significance in the difference attenuation coefficients for these two regions (based on [PIC]:[BSi])? It could be worth plotting regression lines in figure 10b, for only diatom-dominated and only coccolithophore-dominated regions. The plot suggests that there would be no relationship between attenuation coefficient and %>51 μm POC for coccolithophore- dominated regions.

According to the Student's *t*-test, attenuation coefficients at stations with >51 µm [PIC]:[BSi]>1 at z_{PAR} are not significantly different from attenuation coefficients at stations with [PIC]:[BSi]<1. The reviewer is correct that there is no significant correlation between attenuation coefficient and % >51 µm [POC] at z_{PAR} for stations where [PIC]:[BSi]>1, which is why we choose to represent the natural log of [PIC]:[BSi] as a colorbar in Fig. 10 rather than an axis. We find this color bar representation useful for highlighting where particular stations with relatively more >51 µm [PIC] than [BSi] at z_{PAR}, and vice-versa, would fall along the axes in panels a and b. As we elaborate in Sect. 4.7, the information from the color bar points to some relationship between phytoplankton community composition and the attenuation of >51 µm [POC] in the mesopelagic zone.

Comment 21. Page 2879, line 12-23: Could the differences in dissolution rates of PIC and BSi explain the differences in attenuation for the regions dominated by diatoms vs coccolithophores?

Yes, differences in dissolution rates of the two biominerals could confound the relationships we discuss in Fig. 10. But, as stated on page 2870, lines 17-20, there was no association between the magnitude of >51 μm [PIC]:[BSi] change with depth and attenuation. If different dissolution rates systematically biased the relationships in Fig. 10, then we would expect attenuation to scale with these changes in biomineral ratios with depth.

Comment 22. Page 2879, line 21: [PIC]: [Si], should be [BSi]?

Changed on page 2870, line 12.

Comment 23. Table 2: Is b calculated from Zpar to Zpar + 100, or deeper? Is it calculated from > 2 data points? Does the deep transfer efficiency (e.g. POC at ~800m/POC at Zpar) add anything useful to the discussion? Does 'no fit' mean that the fit was not statistically significant? At what level?

The attenuation coefficient, or b-value, is calculated from z_{PAR} to the deepest >51 μm [POC] measurement (800-1000 m), which includes more than two points. We added a clarification to page 2850, lines 2-6. In addition, we added a footnote to Table 2 explaining that no fit means that the Martin curve fit was not statistically significant ($p>0.05$).

It is not possible to calculate a deep transfer efficiency in terms of POC fluxes because ^{234}Th-derived POC flux calculations do not extend to 800 – 1000 m, as there were no ^{234}Th-^{238}U disequilibria at such depths. In terms of concentration, the quotient >51 μm [POC] at 800 m/[POC] at z_{PAR} is analogous and significantly correlated to the attenuation coefficient ($p=1E-05$, $r^2=0.67$). Therefore, b values are sufficient for the purposes of our discussion, and it is not necessary to add another "deep transfer efficiency" metric.

Comment 24. Figures 1, 5, 6 and 8: Would it be possible to use more precise front positions e.g. Orsi et al 1995, Thorpe et al. 2002?

We recognize that the single latitude front positions we've drawn in figures 1, 5, 6, 8 are extremely simplistic, and that a more nuanced categorization based on more

hydrographic parameters would be far more accurate. However, Fig. 1 shows surface temperature relative to our simplistic Subtropical, Subantarctic and Polar front positions, and it can be seen that these provide a reasonable grouping of stations by temperature range. As we primarily use these front positions as a way to facilitate data description in Sect. 3 (pages 2855-2856) and Table 4, we decided to keep our simplistic zonations.

Comment 25. Figures 5-8: Is it area or diameter of circle which corresponds to flux? Difficult to see spatial trends from these figures.

We have included some text in the Figs. 5-8 captions to clarify that the area of the circle corresponds to the value displayed in the legend. We find that this is best geographical representation of the different measurements we discuss in the manuscript. More precise values of these measurements are provided in Tables 2 and 3.

Comment 26. Figure 2: I found it very hard to distinguish the different particle types in this photos – possible just the quality of my printout!

In an attempt to improve the image quality, we imported the images as .tif-files into Adobe Photoshop and applied various image quality adjustments (i.e., sharpening and contrast) and saved them together as an .eps-file. The image is still quite pixelated despite these improvements, but this is the best improvement that is possible with the images that we have. We will re-submit this improved image as Fig. 2, and have shown it above the Fig. 2 caption in the appended track changes section of this response below.

We have added some text in the Fig. 2 caption to direct readers to specific important features in the different panels (e.g., cylindrical fecal pellets in panel c).

Comment 27. Figure 4: very long, lots of info, and not sure it's needed in the main text – could this be moved to supplementary?

We have decided to keep Fig. 4 in the main text because it plays a large role in the results and discussion sections of the manuscript. In particular, we discuss the ^{234}Th activity profiles extensively (Sect. 3 and Sect. 4.1) to assess how the choice of export

depth (z_{PAR} vs. $z_{Th/U}$) impacts the ^{234}Th-derived fluxes we report in the rest of the results/discussion.

Comment 28. Figure 9B and 10B: the regressions seem to be very much driven by station GB1-85 which appears to be an outlier. Did the authors test whether the relationships remain statistically significant if this data point was excluded?

In Fig. 9b, the relationship remains statistically significant if GB1-85 is removed from the regression, as discussed on page 2864, line 10. Likewise, in Fig. 10b, the correlation remains significant ($p<<0.05$) when excluding GB1-85, as discussed on page 2866, lines 20 - 21.

Tracked Changes in Main Text

Abstract

Sequestration of carbon by the marine biological pump depends on the processes that alter, remineralize and preserve particulate organic carbon (POC) during transit to the deep ocean. Here, we present data collected from the Great Calcite Belt, a calcite-rich band across the Southern Ocean surface, to compare the transformation of POC in the euphotic and mesopelagic zones of the water column. The ^{234}Th-derived export fluxes and size-fractionated concentrations of POC, particulate inorganic carbon (PIC), and biogenic silica (BSi) were measured from the upper 1000 m of 27 stations across the Atlantic and Indian sectors of the Great Calcite Belt. POC export out of the euphotic zone was correlated with BSi export. PIC export was not, but did correlate positively with POC flux transfer efficiency. Moreover, regions of high BSi concentrations, which corresponded to regions with proportionally larger particles, exhibited higher attenuation of >51 μm POC concentrations in the mesopelagic zone. The interplay among POC size partitioning, mineral composition and POC attenuation suggests a more fundamental driver of POC transfer through both depth regimes in the Great Calcite Belt. In particular, we argue that diatom-rich communities produce large and labile POC aggregates, which generate high export fluxes but also drive more remineralization in the mesopelagic zone. We observe the opposite in communities with smaller calcifying phytoplankton, such as coccolithophores. We hypothesize that these differences are influenced by inherent differences in the lability of POC exported by different phytoplankton communities.

Sarah Rosengard 5/20/15 5:49 PM
Deleted: dominated

1 Introduction

The biological pump sequesters atmospheric carbon dioxide (CO_2) in the ocean (Volk and Hoffert, 1985) by way of phytoplankton-driven CO_2 fixation, followed by the sinking of this fixed particulate organic carbon (POC) as aggregates and fecal pellets down the water column (Riley et al., 2012). The quantity per unit area and time of POC exiting the base of the euphotic zone defines the export flux, while export efficiency represents the fraction of bulk primary production comprising this flux (Buesseler, 1998). In the mesopelagic zone (from the base of the euphotic zone to ~1000 m), export flux attenuates due to remineralization mediated by zooplankton grazing and bacteria (Buesseler and Boyd, 2009; Giering et al., 2014; Martin et al., 1987). The flux of this processed organic carbon leaving the mesopelagic zone, only ≤10% of export flux, directly scales with the quantity of atmospheric CO_2 sequestered by the marine biological pump over hundreds to thousands of years (Kwon et al. 2009).

On average, only ~1% of the organic matter produced by phytoplankton in the surface reaches the deep sea (Martin et al., 1987). However, export and sequestration flux vary widely by region, as do export efficiencies and attenuation of export flux (Buesseler and Boyd, 2009; Buesseler et al., 2007; Henson et al., 2012b; Henson et al., 2011; Martin et al., 1987; Thomalla et al., 2008). Such variations may drive observed differences in the weight percent of organic carbon deposited at the sediment surface (Hedges and Oades, 1997), suggesting that the overall strength of the biological pump as a carbon sink is not globally uniform. These geographical differences have spurred decades of research into how mechanisms in the shallower ocean – the euphotic and mesopelagic zones – alter sinking particulate organic matter during vertical transit.

As an example, Armstrong et al. (2002), Klaas and Archer (2002) and Francois et al. (2002) posited that mineral associations with sinking organic carbon could explain these variations. Their ballast hypothesis model suggested that minerals enhanced the biological pump (1) by increasing the density, and consequently, the sinking speed of particulate organic matter and (2) by inhibiting organic carbon remineralization down the water column. Expediting vertical transit decreases the time for remineralization to act on sinking particulate organic matter, increasing its chances of reaching the deep sea. The

Sarah Rosengard 5/18/15 11:39 AM
Deleted: ~1000 m below

Sarah Rosengard 5/18/15 11:39 AM
Deleted: remaining intact on its way down

authors observed that calcite flux in the bathypelagic zone (>1000 m) explains roughly half of the variation in the magnitude of POC flux reaching the deep sea (Klaas and Archer, 2002), and may also account for some of the observed geographical variation in POC flux attenuation with depth (Francois et al., 2002).

In its conception and infancy, the ballast hypothesis was based upon observed correlations between mineral and organic carbon fluxes in the deep (>1000 m) sea. Yet, evidence for the ballast mechanism in the euphotic and mesopelagic zones remains equivocal, as deeper correlations are scarcely matched by shallower ocean observations (Le Moigne et al., 2012). Several surface regions do not exhibit ballast correlations between mineral flux and POC flux (e.g., Thomalla et al., 2008; Henson et al., 2012b). In the Atlantic and Southern Oceans, Le Moigne et al. (2012) found a significant fraction of POC export flux to remain unassociated with minerals altogether. Moreover, tank incubations simulating POC and mineral suspensions yield conflicting results: some have observed mineral associations to increase aggregate sinking rates (Engel et al., 2009), while others find no such effect (Passow and De la Rocha, 2006). De La Rocha et al. (2008) even suggest that sticky polymers from POC might ballast sinking minerals, rather than vice-versa.

The scarcity of evidence supporting a shallow ocean ballast mechanism suggests that the transit of particulate organic carbon in the surface, mesopelagic and deeper ocean is mechanistically de-coupled (Lam et al., 2011; Lomas et al., 2010). Indeed, the debate surrounding the ballast hypothesis arises from a deeper issue of whether the mechanisms that influence carbon export from the euphotic zone are the same as those that control its remineralization in the mesopelagic zone, and/or its transfer beyond the mesopelagic zone into the deep sea.

The following report compares the export of organic carbon from the euphotic zone with its transfer through the mesopelagic zone across the region of the Great Calcite Belt (Balch et al., 2011a; Balch et al., 2014; Fig. 1). Spanning across the Southern Ocean, particularly between the Subtropical and Polar Fronts, the Great Calcite Belt defines a highly reflective band observed from space during each austral spring and summer. Its high reflectivity is caused by calcite-rich surface waters produced by coccolithophore blooms in the Southern Ocean. In this zone, coccolithophores are more abundant than in

409 regions north and south of the Belt. South of the Polar Front, coccolithophore abundances
410 decline dramatically as dissolved silica concentrations increase and diatoms flourish
411 (Balch et al., 2011a).
412 Spanning a large range in surface mineral concentrations, primary productivity,
413 and phytoplankton community composition (Balch et al., 2011a), the Great Calcite Belt
414 provides an excellent opportunity to assess the processes controlling organic carbon
415 export, export efficiency, and attenuation of POC concentration ([POC]) with depth.
416 Here, we report estimates of ^{234}Th-derived POC fluxes and [POC] through both the
417 euphotic and mesopelagic zones within the Atlantic and Indian sectors of the Great
418 Calcite Belt. We focus on the upper 1000 m of the Great Calcite Belt because the
419 attenuation of POC flux and concentration is most dramatic within this depth interval
420 (Martin et al., 1987; Lam et al., 2011). As the following discussion illuminates, this study
421 additionally weighs the ballast hypothesis against other mechanisms hypothesized to
422 control the transfer of organic carbon through the water column, and ultimately into the
423 deep sea, where carbon residence time modulates atmospheric pCO_2 and climate over
424 hundreds to thousands of years (Kwon et al., 2009).
425
426 **2 Methods**
427
428 **2.1 Field site**
429
430 Samples from the Great Calcite Belt were collected during two research cruises,
431 GB1 and GB2, which transited the Atlantic and Indian sectors of the Great Calcite Belt
432 during the austral summer of 2011 and 2012, respectively (Fig. 1), concurrent with the
433 putative coccolithophore bloom (Balch et al., 2011a). In 2011, for cruise GB1 (MV1101),
434 the *R/V Melville* crossed the Atlantic sector from Punta Arenas, Chile to Cape Town,
435 South Africa, sampling between 39°S and 59°S. One year later, for cruise GB2
436 (RR1202), the *R/V Revelle* crossed the Indian sector from Durban, South Africa to Perth,
437 Australia, sampling between 37°S and 60°S (Table 1). Both cruise tracks crossed the
438 Subtropical, Subantarctic and Polar fronts, which are approximately located at 40°S, 45°S

and 52°S (e.g., Belkin and Gordon, 1996; Sokolov and Rintoul, 2009), respectively, defining observed shifts in temperature and nutrient characteristics of the surface ocean.

Each day during GB1 and GB2, 30-L Niskin samples were collected pre-dawn for measuring primary production. A Biospherical Instruments (San Diego, CA) sensor was mounted on the CTD/rosette and referenced to a deck sensor mounted on the ship's superstructure to measure Photosynthetically Available Radiation (PAR) during the casts. Water was then sampled at fixed light depths relative to surface irradiance to match light levels in deck-board incubators: 36.5%, 21.1%, 11.7%, 3.55%, 1.93% and 0.28%. The light depths were calculated two ways: (a) between 10:00 and 14:00 h local time (during daylight hours), percentages of surface irradiance were derived directly from the downcast PAR profile immediately preceding bottle firing, or (b) at all other times, the light levels were back-calculated from the previously-determined relationship between beam transmittance and diffuse attenuation of PAR (Balch et al., 2011b). From these casts, primary production rates were measured using the ^{14}C microdiffusion technique (Paasche and Brubak, 1994) with modifications by Balch et al. (2000) (see also (Fabry and Balch, 2010).

2.2 Size-fractionated particle collection

We report measurements of total and particulate ^{234}Th activity and size-fractionated particle composition from 27 stations (Fig. 1; Table 1).

Size-fractionated particles were collected at eight depths in the upper 1000 m of fourteen stations from GB1 and thirteen stations from GB2, using modified battery operated in-situ pumps (McLane WTS-LV). The modified pumps directed seawater through two flow paths (Lam et al., 2014), each of which passed through a "mini-MULVFS" filter holder designed to retain large particles (Bishop et al., 2012). Seawater first passed through 51 µm polyester pre-filters in both filter holders for collection of large (>51 µm) size-fraction particles, and then through paired 0.8 µm polyethersulfone (Supor™) filters in one flow path and paired 1 µm quartz fiber (Whatman™ QMA) filters in the other flow path, both of which collected small (<51 µm) size-fraction particles. An average of 200 L and 500 L of seawater passed through the Supor and QMA

Sarah Rosengard 5/21/15 3:02 PM
Deleted: A

flow paths over 1-2.5 hours, respectively. Immediately after collection, half to all of the >51 µm size-fraction particles from one flow path were rinsed off of the polyester pre-filters and onto 25 mm 1 µm Sterlitech silver filters using 0.2 µm-filtered seawater, and dried at 50°C for subsequent analysis of particulate ^{234}Th, particulate organic carbon (POC), and particulate inorganic carbon (PIC, or calcium carbonate). Subsamples of QMA filters were likewise dried at 50°C for ^{234}Th and POC analysis in the <51 µm size-fraction. Finally, the polyester pre-filters from the other flow path and Supor filters were dried in a laminar flow hood at room temperature.

In the euphotic zone, where most POC is produced, these operationally defined size fractions allude primarily to the structure of phytoplankton communities producing POC (e.g., large diatoms would be found in >51 µm size-fraction particles). In the mesopelagic zone, which extends from the base of the euphotic zone to 1000 m in depth, >51 µm POC is predominantly comprised of phytoplankton and bacterial biomass that has been repackaged into aggregates and fecal pellets. The >51 µm particles collected at station GB1- 85 illustrate these different size-fraction interpretations by depth. Shallower particles collected at 25 m and 73 m, the base of the euphotic zone, are mainly comprised of intact phytoplankton cells (Figs. 2a, 2b). By contrast, deeper particles collected at 173 m exhibit the features of particulate aggregates and fecal pellets (Fig. 2c).

2.3 Particle composition

Bulk concentrations of POC, PIC, biogenic silica (BSi), and particulate ^{234}Th activity were measured in both <51 µm and >51 µm fractions of particles collected at each station. POC concentrations and ^{234}Th activities were measured at all depths of the profiles, while [PIC] and [BSi] were mainly measured at select depths above 200 m and at the deepest depth (800-1000 m) of the profile. Particulate ^{234}Th activities in all sub-fractions of >51 µm (25 mm silver filters) and <51 µm (25 mm QMA filters) samples were measured using low level Risø beta counters immediately on the ship and in the lab at least six ^{234}Th half-lives post-collection for background activity.

After counting for ^{234}Th background activity, ~25% of the silver filter (~ 115 L equivalent) was fumed overnight (12-17 hours) with concentrated hydrochloric acid to

Sarah Rosengard 5/21/15 3:02 PM
Deleted: o

Sarah Rosengard 5/21/15 9:32 AM
Deleted: and depth

Sarah Rosengard 5/21/15 9:32 AM
Deleted:

remove inorganic carbon, before measuring >51 µm [POC] using an elemental CHN analyzer. A similar protocol was followed to measure <51 µm [POC] from one 12 mm-diameter subsample of each QMA filter, representing ~1% of the entire sample (~5 L equivalent). Vertical profiles of >51 µm and <51 µm [POC] between the base of the euphotic zone and the deepest measurement at 800 – 1000 m were fitted to a power-law function to describe the attenuation of [POC] with depth, based on a function first applied to POC flux by Martin et al. (1987) and then analogously to POC concentration by Lam and Bishop (2007),

$$[\mathrm{POC}]_z = [\mathrm{POC}]_0 \left(\frac{z}{z_{PAR}}\right)^{-b} \quad (1)$$

where, at most stations, z_{PAR} represents the depth of 0.3% photosynthetically available radiation (see Sect. 2.4). The exponent b represents the attenuation coefficient, with higher attenuation coefficients (more negative exponents) for profiles with greater attenuation of >51 µm [POC] with depth. We focus our discussion on the attenuation of >51 µm [POC], because we assume that they contribute disproportionately to sinking fluxes compared to the <51 µm size fraction (McCave, 1975; Lam and Bishop, 2007; Lam et al., 2011). Figure 3 and Table 2 show all significant ($p<0.05$) power law fits for >51 µm [POC] profiles.

PIC in the samples was assumed to be biomineral calcium carbonate ($CaCO_3$), and was derived from particulate calcium (Ca) corrected for salt Ca using a seawater 0.0382 Ca:Na (g:g) ratio (Lam and Bishop, 2007; Pilson, 2012). In the in-situ pump samples, salt-derived Ca typically accounted for ~60% of total Ca. The >51 µm PIC size-fraction concentrations were measured mainly in subsamples of remaining pre-filter material and occasionally in sub-fractions of the silver filters, if the former were unavailable. The <51 µm size fraction [PIC] was measured in three 12mm circular QMA subsamples, representing ~15 L or ~3% of the sample. Subsamples were leached in 0.6 N ultrapure Sea-Star™ Baseline hydrochloric acid (HCl) at 60°C for 12-16 hours. The leachate was subsequently filtered through a 0.4 µm polycarbonate membrane filter, diluted to 0.12 N HCl, and spiked with 1 ppb of Indium as an internal standard. The spiked leachate solution was then analyzed for Ca, Na and P using an Element 2 sector-field inductively-coupled plasma mass spectrometer (ICP-MS) in medium and high

Sarah Rosengard 5/18/15 10:41 PM
Deleted: below

Sarah Rosengard 5/20/15 3:01 PM
Deleted: active

resolution. Counts per second were converted to concentration using external mixed element standard curves.

For measuring >51 μm and <51 μm [BSi], prefilter or Supor subsamples, respectively, were leached in 0.2 N sodium hydroxide at 85°C for one hour, and analyzed by standard spectrophotometric detection of the blue silico-molybdate complex in each leachate within 24 hours of the leach (Strickland and Parsons, 1968; Brzezinski and Nelson, 1989). Absorbance through each sample was converted to concentration using an external Si standard curve.

2.4 ^{234}Th-derived flux estimates

Particle fluxes were estimated at each station by measuring the water-column disequilibrium between ^{234}Th and ^{238}U in the upper 350 m of the water-column (Savoye et al., 2006). ^{234}Th is the radioactive daughter of ^{238}U with a short enough half-life (24.1 days) relative to ^{238}U such that it is assumed to be in secular equilibrium with its parent isotope in the absence of particle scavenging (i.e., ^{234}Th activity = ^{238}U activity). Disequilibria between the two isotope activities in the water column are attributed to the scavenging of ^{234}Th by sinking particles (Savoye et al., 2006). Integrating the deficit in ^{234}Th relative to ^{238}U provides a measure of particle flux down the water column (Buesseler et al., 2006). Because of the short half-life of ^{234}Th, deviation from secular equilibrium exists only in regions of high particle flux. Thus, ^{234}Th-based flux estimates are most frequently applied in the euphotic zone of the ocean where particle export is maximal.

^{234}Th-^{238}U deficits were determined by measuring total water-column activities of both isotopes. ^{238}U activity ($A_{U\text{-}238}$) profiles were calculated from salinity by the following relationship (Owens et al., 2011):

$$A_{U-238}\left(\frac{\text{dpm}}{\text{L}}\right) = (0.0786 \times \text{Salinity}) - 0.315 \qquad (2)$$

Total water-column ^{234}Th activity ($A_{Th\text{-}234}$) profiles were determined from 4 L seawater samples collected by CTD casts down to 300-350 m at each station (Pike et al., 2005). Shortly after collection, each 4 L seawater sample was acidified to pH 2 using concentrated nitric acid (HNO_3), spiked with 1 g of ^{230}Th of a known activity (50.06 dpm

568 g^{-1}) as a yield monitor, equilibrated for 8 hours, and finally brought up to pH 8.5 using
569 ammonium hydroxide (NH_4OH) (van der Loeff et al., 2006). Manganese chloride
570 ($MnCl_2$) and potassium permanganate ($KMnO_4$) were added to the neutralized seawater
571 to form a manganese oxide (MnO_2) precipitate, which efficiently scavenges both natural
572 ^{234}Th and added ^{230}Th. After 12 hours, the precipitate was filtered onto a quartz fiber
573 filter, dried at 50°C, and then mounted beneath a sheet of Mylar and aluminum foil. ^{234}Th
574 activity in the precipitate was measured on board by low level Risø beta counters and
575 post-cruise after at least six ^{234}Th half-lives for background activity. The ^{230}Th spike was
576 recovered by fully dissolving the MnO_2 precipitate, adding a 1 g spike of ^{229}Th of a
577 known activity (69.74 dpm g^{-1}), and measuring ^{229}Th:^{230}Th ratios on an Element 2 sector-
578 field ICP-MS in low resolution. Recovery of ^{230}Th spike was derived from this ratio, and
579 used to correct for inefficiencies in the scavenging of total seawater ^{234}Th by MnO_2
580 precipitation.
581 To calibrate beta counting efficiency for each cruise, total deep water (i.e., below
582 2000 m) ^{234}Th activities were compared to total deep water ^{238}U activities, as measured in
583 4-5 replicate samples from 2-3 deep water CTD casts during each cruise (at 5000 m
584 during GB1, and at 2500 m during GB2). Beta counting efficiencies were adjusted such
585 that ^{234}Th and ^{238}U activities were equal in these deep measurements, as secular
586 equilibrium would be expected at such depths. We only report upper water-column
587 activities (<350 m) after correcting for experimental efficiencies in both the seawater
588 collection process and beta detector counting. Uncertainties in the total ^{234}Th activity
589 profiles averaged 4.5% and were propagated from errors associated with counting
590 statistics, recoveries, and beta-counting efficiency.
591 To calculate ^{234}Th export flux, ^{234}Th activity deficits were integrated down to the
592 base of the euphotic zone (z_{PAR}) (Buesseler et al., 2008; Thomalla et al., 2008):

593 $$^{234}\text{Th Flux}\left(\frac{\text{dpm}}{\text{m}^2\text{d}}\right) = \int_0^{z_{PAR}} (A_{\text{U}-238} - A_{\text{Th}-234})\, dz \qquad (3)$$

594 At most stations, the export depth, z_{PAR}, was chosen to be the depth where light
595 levels were 0.3% of surface-level PAR. The exception was station GB2-27, which did not
596 include a PAR measurement profile. For this station, the z_{PAR} value of 105 m was defined
597 as the depth where the transmissometry-based particle concentration decreased. These
598 export depths were compared to one additional metric describing particle concentration in

599 seawater: the depths where ^{234}Th and ^{238}U activities re-established secular equilibrium, or
600 $z_{Th/U}$. We explore the sensitivity of ^{234}Th flux estimates to choice of z_{PAR} in Sects. 3 and
601 4.1.
602 ^{234}Th flux estimates were converted to POC, PIC and BSi fluxes by multiplication
603 with ratios of >51 μm POC, PIC, and BSi concentrations to particulate ^{234}Th activity in
604 samples at z_{PAR} (Thomalla et al., 2008; Sanders et al., 2010):

605 $$\text{POC Flux}\left(\frac{\text{umol}}{\text{m}^2\text{d}}\right) = [\text{POC}]: A_{\text{Th}-234} \times {}^{234}\text{Th Flux}\left(\frac{\text{dpm}}{\text{m}^2\text{d}}\right) \quad (4)$$

606 $$\text{PIC Flux}\left(\frac{\text{umol}}{\text{m}^2\text{d}}\right) = [\text{PIC}]: A_{\text{Th}-234} \times {}^{234}\text{Th Flux}\left(\frac{\text{dpm}}{\text{m}^2\text{d}}\right) \quad (5)$$

607 $$\text{Si Flux}\left(\frac{\text{umol}}{\text{m}^2\text{d}}\right) = [\text{BSi}]: A_{\text{Th}-234} \times {}^{234}\text{Th Flux}\left(\frac{\text{dpm}}{\text{m}^2\text{d}}\right) \quad (6)$$

608

609 **2.5 Interpolation of data**

610

611 In all cases where ^{234}Th activity, >51 μm and <51 μm [POC] and mineral
612 concentrations, and >51 μm particulate ^{234}Th measurements were unavailable at z_{PAR},
613 linear interpolations between the sampling depths above and below z_{PAR} were used to
614 estimate a value at the export depth (Table 1). The >51 μm and <51 μm size-fraction
615 POC concentrations were interpolated by the power law attenuation function when fits
616 were significant ($p<0.05$), or linearly when these power-law fits were not significant or
617 inconsistent with the broader shape of the [POC] profile at that particular station. In
618 general, corresponding POC:^{234}Th, BSi:^{234}Th, and PIC:^{234}Th ratios are quotients of these
619 interpolated values except as noted in Tables 2 and 3.

620

621 **3 Results**

622

623 ^{234}Th activity profiles were measured over the upper 300 – 350 m at the 27
624 stations of cruises GB1 and GB2 (Fig. 4; Table S1). Each activity profile is associated
625 with two metrics that have been used in previous studies to define the export depth (see
626 Sect. 2.4): the base of the euphotic zone (z_{PAR}), which we define at 0.3% surface
627 photosynthetically available radiation (PAR) (e.g., Buesseler and Boyd 2009), and $z_{Th/U}$,
628 where ^{234}Th and ^{238}U activities re-establish secular equilibrium (Table 1). In most

stations, profiles exhibited ^{234}Th activity deficits over a range from surface to 75 – 170 m in depth, below which ^{234}Th activity generally returned to secular equilibrium with ^{238}U activity, within error. The notable exceptions were profiles at stations GB1-6, and GB1-16, which did not return to secular equilibrium by 170 m in depth. Considering that stations GB1-6 and GB1-16 are closest to shore, their sustained ^{234}Th deficits may have been influenced by lateral advection of particles from the continental shelf. At these stations, $z_{Th/U}$ depths were approximated by the depth below which ^{234}Th activities remain constant with depth. For example, at station GB1-6, $z_{Th/U}$ = 130 m because below this depth ^{234}Th activities remained relatively constant.

In the Atlantic sector, sampled in January – February 2011, all observed z_{PAR} depths were significantly shallower than $z_{Th/U}$ depths (Student's t-test $p<0.05$); on average, z_{PAR} was 66 ± 44 % shallower than $z_{Th/U}$. By contrast, in the Indian sector, sampled roughly a year later in February – March 2012, z_{PAR} was not significantly different from $z_{Th/U}$ ($p>0.05$), and the average relative difference was -6 ± 29%. In general, when water-column ^{234}Th activity is at steady-state, the euphotic zone should correspond to the region of ^{234}Th deficit relative to ^{238}U (Buesseler et al., 2008; Buesseler and Boyd, 2009), i.e., z_{PAR} should equal $z_{Th/U}$.

Using integrated activity deficits, export fluxes of ^{234}Th, POC, PIC, and BSi at z_{PAR} were estimated at the 27 sites (Figs. 5, 6; Table 3). Overall mean ^{234}Th fluxes at z_{PAR} were 1,413 ± 432 dpm m^{-2} d^{-1} (mean ± 1 s.d.), and ranged from 717 to 2,437 dpm m^{-2} d^{-1} at stations GB2-112 and GB1-6, respectively. Mean derived POC fluxes at z_{PAR} were 4.5 ± 3.9 mmol m^{-2} d^{-1}, ranging from 0.97 to 20 mmol m^{-2} d^{-1} at stations GB2-112 and GB1-85, respectively. Mean PIC fluxes were 1.2 ± 1.7 mmol m^{-2} d^{-1}, and ranged from 0.067 to 6.2 mmol m^{-2} d^{-1} at stations GB2-73 and GB1-59, respectively. Finally, mean BSi fluxes at z_{PAR} were 3.8 ± 5.8 mmol m^{-2} d^{-1}, ranging from 0.17 to 28 mmol m^{-2} d^{-1}at stations GB2-46 and GB1-85, respectively. Higher POC export stations frequently corresponded with higher BSi export stations (e.g., station GB1-85), but less so with higher PIC export stations.

The highest and lowest measured biomineral (PIC and BSi) fluxes at z_{PAR} were in GB1 and GB2, respectively, but mean values were not significantly different between ocean basins because of high variability within each basin (Fig. 6). However, mean POC

660 fluxes at z_{PAR} were significantly higher in GB1 (mean ± 1 s.d.= 6.0 ± 4.9 mmol m^{-2} d^{-1})
661 than in GB2 (3.0 ± 1.7 mmol m^{-2} d^{-1}) (Student's t-test $p>0.05$). Because POC:^{234}Th values
662 did not differ between GB1 and GB2 ($p<0.05$), we attribute this inter-basin difference in
663 POC fluxes primarily to significantly higher ^{234}Th fluxes in GB1 (1,574 ± 463 dpm m^{-2} d^{-1})
664 relative to fluxes in GB2 (1,240 ± 330 dpm m^{-2} d^{-1}).
665 Further, there were significant latitudinal differences among export fluxes and
666 particulate composition ratios in three temperature/nutrient regimes across both sectors
667 (Fig.1; Table 4): (1) north of 45° S, the approximate location of the Subantarctic front,
668 where temperatures exceeded ~10°C; (2) south of 52 °S, the approximate location of the
669 Polar Front (e.g., Belkin and Gordon, 1996; Sokolov and Rintoul, 2009), where
670 temperatures remained below ~5°C; and (3) between 45° S and 52 °S, where
671 temperatures ranged from ~5-10 °C. The >51 μm size-fraction POC:^{234}Th values at z_{PAR}
672 were significantly lower in the most equatorward zone north of 45 °S, where average
673 ratios were 1.9 ± 0.9 μmol dpm^{-1}. The highest average ratios, south of 52°S, were 5.4 ±
674 3.0 μmol dpm^{-1}, illustrating the wide variation in POC:^{234}Th ratios with ecosystem type
675 (Buesseler et al., 2006; Jacquet et al., 2011). Likewise, zonally averaged POC export
676 fluxes in the most equatorward zone (2.7 ± 2.3 mmol m^{-2} d^{-1}) were significantly lower
677 than average fluxes in the most poleward zone (8.0 ± 6.3 mmol m^{-2} d^{-1}). BSi:^{234}Th values
678 were significantly different in all three zones, with highest average ratios south of 52°S
679 (7.1 ± 4.1 μmol dpm^{-1}) and smallest ratios north of 45°S (0.3 ± 0.1 μmol dpm^{-1}).
680 Similarly, average BSi export fluxes were also significantly different from each other in
681 all three zones, with the greatest average values south of 52°S (10 ± 8.7 mmol m^{-2} d^{-1}),
682 and lowest values north of 45°S (0.35 ± 0.16 mmol m^{-2} d^{-1}). Finally, PIC:^{234}Th ratios,
683 which averaged 0.72 ± 0.85 μmol dpm^{-1} across all zones, and PIC export fluxes were not
684 significantly different from each other in any zone defined by these latitudinal bands.
685 These fluxes are sensitive to the choice of export depth (z_{PAR} or $z_{Th/U}$), not only
686 because the export depth determines the magnitude of ^{234}Th flux by influencing the
687 integrated ^{234}Th deficit, but also because the export depth determines which POC:^{234}Th
688 ratio best describes particles sinking from the chosen depth (Fig. S1). Across stations, the
689 depth metrics z_{PAR} and $z_{Th/U}$ differed from each other to varying extents (Fig. 4; Table 1).
690 As exemplified by stations GB1-92, GB1-16, and GB2-100, POC fluxes changed

691 significantly between z_{PAR} and $z_{Th/U}$ (Figs. 5b, 5c; Table S2). At station GB1-92, where
692 z_{PAR} was 40 m shallower than $z_{Th/U}$, POC flux decreased from 8.0 mmol m^{-2} d^{-1} at z_{PAR} to
693 5.1 mmol m^{-2} d^{-1} at $z_{Th/U}$. In contrast, at station GB1-16, where z_{PAR} was 80 m shallower
694 than $z_{Th/U}$, POC fluxes increased from 5.9 mmol m^{-2} d^{-1} to 6.6 mmol m^{-2} d^{-1}. At station
695 GB2-100, one of few stations where z_{PAR} was deeper than $z_{Th/U}$, POC fluxes decreased
696 from 3.3 to 1.5 mmol m^{-2} d^{-1} going deeper. At this station, the POC:^{234}Th ratio at $z_{Th/U}$
697 was 102% greater than ratios at z_{PAR}, while ^{234}Th fluxes at $z_{Th/U}$ were 6% greater than
698 fluxes at z_{PAR}, demonstrating that changes in particle composition disproportionately
699 contributed to the observed difference in POC export at z_{PAR} and $z_{Th/U}$. By contrast, at
700 station GB1-16, the relative change in ^{234}Th fluxes from z_{PAR} to $z_{Th/U}$ (+29%) contributed
701 more to the increase in POC flux with depth than the relative change in POC:^{234}Th ratio
702 (-13%). Finally, for station GB1-92, the relative change in ^{234}Th flux with depth (-19%)
703 was similar to the relative change in POC:^{234}Th with depth (-21%), demonstrating that
704 the export flux estimate was equally sensitive to changes in both parameters.
705
706 **4 Discussion**
707
708 The following discusses these flux measurements in the context of other Southern
709 Ocean observations, and hypotheses surrounding the transformation of sinking organic
710 carbon within the euphotic and mesopelagic zones of the water column.
711
712 **4.1 Choice of export depth**
713
714 The two possible depths we use to calculate export flux, z_{PAR} and $z_{Th/U}$, are
715 significantly different in the Atlantic sector, which influences the magnitude of flux
716 estimated (see Sect. 3). We offer here two possible and not mutually exclusive
717 explanations for why $z_{Th/U}$ depths were on average deeper than z_{PAR} depths at GB1
718 stations.
719 One hypothesis is that the ^{234}Th - ^{238}U profiles used to calculate export fluxes may
720 not have been at steady-state during the time of sampling on the GB1 cruise. Non-steady
721 state conditions in the ^{238}U-^{234}Th system do occur during phytoplankton blooms,

particularly during their decline and ascent (Savoye et al., 2006; Buesseler et al., 2009). For example, a recent and rapid increase in the near-surface particle concentration could decrease the depth of light penetration faster than the ^{238}U-^{234}Th system can adjust, leading to a z_{PAR} measured on station that is shallower than the $z_{Th/U}$, which reflects conditions prior to the rapid increase. Since the GB1 cruise in the Atlantic sector took place a month earlier in the growing season (January-February 2011) than the GB2 cruise in the Indian sector (February-March 2012), the two sectors may have been sampled at different stages of the seasonal bloom, contributing to differences in agreement between z_{PAR} and $z_{Th/U}$. Satellite chlorophyll time-series, if well-resolved, can shed light on how dynamic primary production was around the time of sampling at each station of GB1 and GB2, whether rapid (i.e., within three weeks) changes in particle production and sinking fluxes from a bloom could have decoupled ^{234}Th-^{238}U deficits from light profiles into the surface ocean of the Great Calcite Belt. Eight-day composites of chlorophyll imagery from December 2010 to February 2011 were required to overcome spatial patchiness in the data due to clouds, and indicate that the changes leading up to sampling during GB1 were not consistent across all stations where $z_{PAR} < z_{Th/U}$. At several stations, chlorophyll concentrations declined towards the sampling date; at others, chlorophyll did not change or increased towards the sampling date. Moreover, out of the three stations where $z_{PAR} = z_{Th/U}$, only one exhibited relatively constant chlorophyll concentrations in the month preceding sampling. In GB2, where the differences between z_{PAR} and $z_{Th/U}$ were not significant, chlorophyll tended to be constant preceding more sampling stations. Nonetheless, as in GB1, several locations still experienced increasing or decreasing chlorophyll concentrations in the weeks before sampling, despite having a similar z_{PAR} and $z_{Th/U}$.

The inability of the chlorophyll time-series to unequivocally resolve the differences between z_{PAR} and $z_{Th/U}$ points to other possible mechanisms underlying the discrepancy. One other mechanism, which does not necessarily preclude non-steady state in the ^{234}Th system, is sinking particle production below the euphotic zone z_{PAR} (Trull et al., 2008). Physical aggregation and fecal pellet production by zooplankton grazing in the region below z_{PAR} (i.e., the upper mesopelagic zone) can increase the speed and total abundance of sinking of particles by transforming phytoplankton biomass exiting the

Sarah Rosengard 5/18/15 1:58 PM
Deleted: time-series

Sarah Rosengard 5/21/15 9:36 AM
Deleted: productivity

Sarah Rosengard 5/21/15 9:36 AM
Deleted: productivity

Sarah Rosengard 5/18/15 2:02 PM
Deleted: experienced

Sarah Rosengard 5/18/15 2:02 PM
Deleted: primary productivity

Sarah Rosengard 5/21/15 9:37 AM
Deleted: primary productivity

Sarah Rosengard 5/21/15 9:37 AM
Deleted: productivity

euphotic zone, thereby contributing to sustained ^{234}Th deficits below z_{PAR} (Steinberg et al., 2008; Wilson et al., 2008; Abramson et al., 2010). Why this occurs only in GB1 and not GB2 is not known.

For example, the ~70m difference in z_{PAR} and $z_{Th/U}$ at a station like GB1-85 (Table 1) may be attributed to additional production or repackaging of sinking particles in the upper mesopelagic zone, causing ^{234}Th deficits to persist beyond the euphotic zone of primary productivity, and a deeper $z_{Th/U}$. Images of >51 µm particles from this station highlight the changing nature of >51 µm particles with depth (Fig. 2), from primarily large phytoplankton in the euphotic zone to predominantly fecal pellets in the mesopelagic zone. The difference in POC fluxes measured at both depths may arise from the evolution of these particles during vertical transit, from predominantly intact and relative buoyant diatoms at z_{PAR} to degraded, sinking fecal pellets produced between z_{PAR} and $z_{Th/U}$.

Going forward, it is most important to keep in mind how the choice of export depth impacts flux estimates. For this study, all export fluxes are defined by z_{PAR} so that they can be compared with integrated primary production measurements (Buesseler and Boyd, 2009). Non-steady-state effects of ^{234}Th profiles on export fluxes will not be considered further because we do not have Lagrangian observations at multiple time points necessary to detect such effects (Buesseler et al., 2003; Resplandy et al., 2012).

4.2 Comparison of export fluxes to previous studies

The ^{234}Th fluxes we report (mean ± S.D.= 1,413 ± 432 dpm m^{-2} d^{-1}) are generally within range of measurements from other Southern Ocean studies (1,615 ± 1,050 dpm m^{-2} d^{-1}) (compilation by Le Moigne et al., 2013; Shimmield et al., 1995; Rutgers Van Der Loeff et al., 1997; Buesseler, 1998; Cochran et al., 2000; Buesseler et al., 2001; Friedrich and van der Loeff, 2002; Buesseler et al., 2003; Coppola et al., 2005; Morris et al., 2007; Thomalla et al., 2008; Savoye et al., 2008; Rodriguez y Baena et al., 2008; Jacquet et al., 2011; Rutgers van der Loeff et al., 2011; Zhou et al., 2012; Planchon et al., 2013). By contrast, the POC fluxes we report (4.5 ± 3.9 mmol m^{-2} d^{-1}) are on average three times lower than fluxes from other studies (12.6 ± 13.3 mmol m^{-2} d^{-1}) due to lower POC:^{234}Th

Sarah Rosengard 5/19/15 12:09 PM
Deleted: e.g.,

Sarah Rosengard 5/19/15 12:01 PM
Deleted: (

Sarah Rosengard 5/19/15 12:09 PM
Deleted: ;

Sarah Rosengard 5/19/15 12:02 PM
Formatted: Superscript

ratios measured in >51 μm particles. In general, POC:^{234}Th ratios can vary widely as a function of season, ecosystem composition, size-fraction, depth, and particle sampling methodology (Coppola et al., 2005; Buesseler et al., 2006; Santschi et al., 2006; Jacquet et al., 2011). In GB1 and GB2, an ecosystem effect likely accounts for the 14-fold difference in POC:^{234}Th between oligotrophic waters (e.g, 0.8 μmol dpm^{-1} at GB2-106) and polar waters (e.g., 10.8 μmol dpm^{-1} at GB1-85) (Table 3). The Le Moigne et al. (2013) dataset may include more studies from diatom-rich ecosystems with high POC:^{234}Th organic particles, such as observed by Buesseler (1998; not included in Le Moigne et al. 2013), driving some of the discrepancy between our observations and POC fluxes reported by (Le Moigne et al., 2012).

Other potential reasons for POC:^{234}Th differences are the choice of export depth (see Sect. 4.1) and different sampling methodologies in the previous studies. For instance, in-situ pump filter holders with a small-diameter central intake and thus higher intake velocities have been observed to sample more zooplankton, which typically have higher POC:^{234}Th ratios, than filter holders with diffuse intakes (Bishop et al., 2012). This is because swimming zooplankton can avoid the gentle intake velocities of filter holders with diffuse intakes but not the higher velocities of small diameter intakes. This would be expected to affect estimates of ^{234}Th-derived POC flux more than ^{234}Th-derived biomineral fluxes.

There have been far fewer estimates of ^{234}Th-derived biomineral export fluxes (Thomalla et al., 2008; Sanders et al., 2010; Le Moigne et al., 2012; Le Moigne et al., 2013). BSi and PIC fluxes observed during GB1 and GB2 are within the range previously observed during the *Crozex* study by the Crozet islands (Le Moigne et al., 2012), the site of station GB2-27. Thomalla et al. (2008) also reported biomineral fluxes from the Atlantic Meridional Transect (AMT), north of the Subantarctic Front. While AMT PIC export fluxes were only two times smaller than our mean PIC fluxes in the Great Calcite Belt region, AMT BSi fluxes were ten times smaller. The disparity in BSi fluxes is unsurprising, since the AMT cruise track was through waters with low abundance of silicifiers. We also find that the PIC and BSi fluxes from our Great Calcite Belt study are 4 and 10 times larger than biomineral fluxes estimated by Henson et al. (2012b), respectively, who used a steady-state model of nutrient uptake against nutrient

825 export (Sarmiento et al., 2002; Sarmiento et al., 2004). The Henson et al. method used
826 annual climatologies of nutrient concentration profiles for their estimates, whereas the
827 ^{234}Th-derived export method used here integrates over several weeks in the growing
828 season. This difference in timescales of integration likely accounts for the smaller
829 biomineral fluxes in Henson et al. (2012b).
830
831 **4.3 Export efficiency**
832
833 We found no significant relationship observed between integrated primary
834 productivity and POC flux at z_{PAR}, highlighting the variable export efficiency across GB1
835 and GB2. Export efficiencies, or "Ez-ratios" (Buesseler and Boyd, 2009), were calculated
836 as the ratio of POC flux at z_{PAR} to total integrated primary production in the euphotic
837 zone (Fig. 7b; Table 3). Mean export efficiencies were 0.26 ± 0.19, and ranged from 0.04
838 to 0.77 at stations GB1-16 and GB2-63, respectively. The lack of association between
839 primary productivity and POC export flux confirms previously observed decoupling
840 between the factors that drive export and those that modulate primary productivity
841 (Buesseler et al., 2001; Coppola et al., 2005; Maiti et al., 2012).
842
843 **4.4 Vertical attenuation of POC flux and concentration**
844
845 At most stations, both POC flux and >51 μm [POC] decline with depth below
846 z_{PAR} as a result of remineralization. In the following, we use two metrics to describe POC
847 transfer in the mesopelagic zone: (1) the attenuation of >51um [POC] in the mesopelagic
848 zone, expressed as the attenuation coefficients extracted from power-law fits of
849 mesopelagic >51 μm [POC] (exponent from Eq. (1)) and (2) the POC flux transfer
850 efficiency (T_{100}), defined as the fraction of ^{234}Th-based POC flux that survives
851 remineralization and is transferred 100 m below z_{PAR} (Buesseler and Boyd, 2009). The
852 first metric describes the disappearance of POC concentration, and applies to the entire
853 mesopelagic zone; the second metric describes the survival of POC flux, and applies to
854 the upper mesopelagic zone.

Sarah Rosengard 5/18/15 3:32 PM
Deleted: 2010

The mean T_{100} was 0.71 ± 0.38, ranging from 0.20 to 1.8 at stations GB2-119 and GB1-25, respectively (Fig. 7c**;** Table 2), generally falling within the spread of values observed globally as well as specifically in the Southern Ocean (Buesseler and Boyd, 2009). At stations GB1-6, GB1-16, GB1-25, GB1-59, and GB2-106, T_{100} values are greater than 1.0 and reflect an increase in POC flux with depth between z_{PAR} and 100 m below z_{PAR} (Figs. 5b, 5d). Transfer efficiencies greater than 1 can occur during a declining bloom (Henson et al., 2015), but examination of satellite chlorophyll time-series does not indicate that these stations were sampled at such conditions. At GB1-6, GB1-16 and GB1-59, the ^{234}Th-^{238}U disequilibrium extends relatively deep (>200m) into the water column, thus leading to continually increasing ^{234}Th flux with depth, suggesting that either renewed particle production at depth or lateral advection of particles away from these coastal stations could sustain the ^{234}Th deficit below z_{PAR}. Moreover, because z_{PAR} depths are significantly shallower than $z_{Th/U}$ in most GB1 stations, including GB1-6, GB1-16 and GB1-59, the transfer efficiency calculation at these stations in GB1 captures an increase in ^{234}Th flux between z_{PAR} and 100 m below z_{PAR}. Thus, for the following discussion, it is important to view transfer efficiency values with the caveat that GB1 and GB2 stations display different ^{234}Th-^{238}U disequilibria profiles with respect to z_{PAR} and $z_{Th/U}$, and this difference impacts all calculations that use a ^{234}Th flux component.

At the two other stations for which T_{100}>1, GB1-25 and GB2-106, the increases in POC flux below z_{PAR} arise primarily from increasing POC:^{234}Th ratios rather than increasing ^{234}Th flux with depth (Figs. S1a, S1d). The increase in these ratios results from a faster decrease in particulate ^{234}Th activity compared to changes in >51 µm [POC] with depth. This is unexpected and at all other stations, >51 µm [POC] decreases more quickly than particulate ^{234}Th activity due to organic carbon remineralization. We suspect that poor >51 µm particle distribution on filters from GB2-106 may have led to anomalously low POC around z_{PAR}, but do not have an explanation for the consistent increase in POC:Th with depth at GB1-25 (Figs. S1a). We proceed by excluding the T_{100} transfer efficiencies from these two stations from statistical tests, but identify them for completeness (Figs. 7, 9).

The general decline in POC flux with depth at most stations is mirrored by a decrease in >51 µm [POC], both of which are a result of remineralization. Attenuation

Sarah Rosengard 5/18/15 5:46 PM
Deleted: where

Sarah Rosengard 5/21/15 9:41 AM
Deleted: a sampling issue and thus exclude

Sarah Rosengard 5/21/15 9:41 AM
Deleted: further consideration

coefficients from power-law fits of mesopelagic >51 μm [POC] at 22 stations describe this transformation from z_{PAR} to the lower mesopelagic zone, where >51 μm [POC] between 800-1000 m was 1.5 to 137 times lower than >51 μm [POC] at z_{PAR} (Figs. 8b, 8c; Table 2). We discount the attenuation value at station GB2-93 from discussion because it had an anomalously low >51 μm [POC] at 800m, likely due to incomplete rinsing of particles from the prefilter. This drove the power law fit to yield an anomalously high attenuation coefficient, an outlier, as approximated by Chauvenet's Theorem (Glover et al., 2011). Attenuation coefficients were 1.1 ± 0.50 on average, and varied from 0.4 to 1.9 at stations GB1-25 and GB2-43, respectively (Fig. 8c; Table 2), which spans the global range compiled by Lam et al. (2011).

The >51 μm [POC] at z_{PAR} is not correlated with >51 μm [POC] at lower mesopelagic depths, suggesting that processes controlling >51 μm [POC] at the top of the mesopelagic differ from those controlling >51 μm [POC] at the base of the mesopelagic zone. This is supported by the great variation in attenuation coefficients and transfer efficiencies, and suggests that POC concentrations at z_{PAR} are decoupled from [POC] at z ≥800m, as has also been noted in other POC flux and concentration observations (Lomas et al., 2010; Lam et al., 2011; Henson et al., 2012b). There are some exceptions, such as at GB1-85, which exhibited the highest >51 μm [POC] both at z_{PAR} and below 800 m, but there is no overall relationship across the dataset. The remaining discussion aims to tease apart the processes that control POC flux and >51 μm [POC] in each depth regime.

4.5 Biomineral-POC flux correlations at z_{PAR}

We compared POC fluxes to mineral fluxes at z_{PAR} (Figs. 9a, 9b) to test the hypothesis that mineral ballasting facilitates POC export out of the euphotic zone, as has been observed in deeper flux datasets >1000 m (Klaas and Archer, 2002; Armstrong et al., 2002; Francois et al., 2002). Because we use ^{234}Th activity deficits and the same particulate ^{234}Th activities to derive all fluxes (Eq. (4-6)), comparing export fluxes is equivalent to comparing concentrations of >51 μm POC, BSi and PIC at z_{PAR}. In this dataset, minor differences between flux versus concentration comparisons (not shown)

arise from differences in interpolation methods for POC:^{234}Th, BSi:^{234}Th, and PIC:^{234}Th ratios at z_{PAR} (Table 3).

Pearson correlation tests between shallow POC export and the two biomineral fluxes revealed a significantly positive correlation between POC and BSi fluxes ($p<<0.001$, $r^2=0.77$). By contrast, there was no significant relationship between shallow POC and PIC fluxes ($p=0.24$, $r^2=0.06$). Both BSi and POC export fluxes tend to increase poleward from the region north of the Subtropical/Subantarctic fronts to the inter-frontal zone to the region south of the Polar front (Figs. 5b, 6a, 6b). Station GB1-85, which sits just south of the Polar Front (~52°S), is a high BSi and POC flux outlier. When removed, the BSi flux vs. POC flux correlation remains significant, though weaker ($r^2= 0.43$), suggesting that although this correlation is strongly influenced by station GB1-85, the shallow BSi ballast association still remains valid for the rest of the dataset.

We also compared POC export fluxes to both PIC and BSi export fluxes simultaneously by multiple linear regression:

$$\text{POC Flux} = (m_{\text{BSi}} \times \text{BSi Flux}) + (m_{\text{PIC}} \times \text{PIC Flux}) + \text{constant} \quad (7)$$

The multiple linear regression only explains an additional 5% of the variance in POC flux at z_{PAR} ($r^2=0.82$, $p<< 0.001$), affirming that BSi flux explains most of the variation in POC export fluxes at z_{PAR} across the Atlantic and Indian sectors of the Great Calcite Belt region.

The per-mole carrying capacities of BSi and PIC for POC, or the slopes m_{BSi} and m_{PIC} in the multiple linear regression Eq. (7), are 0.60 and 0.50, respectively. The per-weight carrying capacities of BSi and PIC for POC are 0.23 and 0.13, respectively, assuming 12 x 2.199 g mol^{-1} POC, 67.3 g $SiO_2 0.4H_2O$ mol^{-1} BSi and 100.1 g $CaCO_3$ mol^{-1} PIC (Klaas and Archer 2002). The unassociated POC flux, the constant in Eq. (7), is 1.7 mmol POC m^{-2} d^{-1}, or 44 mg POC m^{-2} d^{-1}. These carrying capacities for POC are 2-10 times higher than global biomineral carrying capacities of deeper (>2000m) flux data (m_{BSi}=0.025-0.026, m_{PIC}=0.070-0.074; Klaas and Archer, 2002), reflecting how POC remineralization with depth consistently reduces apparent mineral carrying capacities between the base of the euphotic zone and the deep sea.

These upper ocean carrying capacities, especially m_{PIC}, are considerably different than corresponding per-weight carrying capacities reported in the *Crozex* study in the

Sarah Rosengard 5/18/15 6:15 PM
Deleted: , as defined by

Sarah Rosengard 5/18/15 6:16 PM
Deleted: , on a per-mole basis, and

Sarah Rosengard 5/18/15 6:18 PM
Deleted: , on a per-weight basis

Sarah Rosengard 5/18/15 6:22 PM
Deleted:

Sarah Rosengard 5/18/15 6:14 PM
Deleted: x 2.199

Sarah Rosengard 5/18/15 6:15 PM
Deleted: as defined by

957 Indian sector of the Southern Ocean (m_{BSi}= 0.16, m_{PIC}= -0.11, constant=105 mg POC m^{-2}
958 d^{-1}) (Le Moigne et al., 2012). But, as the *Crozex* study was carried out several months
959 earlier in the growing season than our sampling of the same area within the Great Calcite
960 Belt, seasonal changes in the phytoplankton communities and their associated food webs
961 could account for the differences in upper ocean carrying capacities. The Le Moigne et al.
962 (2012) study also highlighted that variable ecosystem composition contributed to regional
963 variations in upper ocean carrying capacities (Le Moigne et al. 2014), echoing a
964 contemporaneous study that showed that even the deep (>1500 m) flux carrying
965 capacities have statistically significant spatial variability (Wilson et al., 2012).
966 It is worth noting that Le Moigne et al. (2012) included lithogenic minerals in
967 their multiple linear regressions. We did not measure lithogenic minerals on GB1 and
968 GB2, as we assumed lithogenic fluxes to be small in the Southern Ocean due to low
969 terrestrial dust inputs (e,g., Honjo et al., 2000). While omitting this lithogenic component
970 from the multiple linear regression could potentially impact derived m_{BSi} and m_{PIC} values,
971 lithogenic material is nonetheless unlikely to be an important carrier of POC flux because
972 of its low flux in the Southern Ocean. Indeed, regional studies have found that the
973 lithogenic carrying capacity (Wilson et al., 2012) and the lithogenic-associated POC
974 fluxes (Le Moigne et al., 2012) are very low in the Southern Ocean.
975
976 **4.6 Mineral-POC flux correlations in the mesopelagic zone**
977
978 To directly test whether minerals facilitate POC transfer through the upper
979 mesopelagic zone of the water column as well, we compared flux transfer efficiencies
980 100 m below the base of the euphotic zone (T_{100}) with BSi and PIC fluxes at z_{PAR} (Figs.
981 9c, 9d). If the mineral ballast model were to apply to the upper mesopelagic zone, one
982 would expect greater transfer efficiencies (i.e., lower attenuation of POC flux) in regions
983 of higher mineral export. The data highlight several key differences between the role of
984 minerals in the euphotic and upper mesopelagic zones. For one, the correlation between
985 PIC flux and T_{100} , excluding values at GB1-25 and GB2-106, is significantly positive
986 ($p<0.001$, $r^2=0.39$). The relationship remains even when assessing data from each cruise

individually (for GB1, p=0.047, r^2= 0.34; for GB2, p= 0.009, r^2=0.52), lending further support to a potential role for PIC in POC transfer through the upper mesopelagic zone.

Further, there was no significant correlation, with or without GB1-25 and GB2-106 T_{100} values, between BSi export fluxes in GB2 and T_{100}. However, higher particulate biogenic silica concentrations (>51 μm [BSi]) at z_{PAR} did correspond with greater attenuation of >51 μm [POC] below z_{PAR} (p=0.004, r^2=0.35; Fig. 10a), suggesting that in contrast to its role in the euphotic zone, BSi is associated with greater degradation in the mesopelagic zone of the water column.

4.7 Other controls on POC transfer

The correlation between the attenuation of >51 μm [POC] and the size fractionation of POC (% >51 μm [POC]) at z_{PAR} is even stronger than with >51 μm [BSi] (p<<0.001, r^2=0.63; Fig. 10b). GB1-85 appears to be an outlier for both relationships in Fig. 10, but especially for the relationship between >51 μm [POC] attenuation and >51 μm [BSi] (Fig. 10a). The correlation remains significant when the high [BSi] value from station GB1-85 is removed. Notably, the power law fit at GB1-85 is not very good in the upper mesopelagic; fitting >51 μm [POC] between z_{PAR} and 500 m yields a better fit (higher r^2; see Fig. 3) with a higher attenuation coefficient of 2.35 (compared to 1.7 for the entire mesopelagic zone). This modified upper mesopelagic attenuation at GB1-85 improves the overall correlations between the attenuation coefficient and both >51 μm [BSi] (p<<0.001, r^2=0.60) and % >51 μm [POC] (p<<0.001 ; r^2=0.78), further strengthening the argument that >51 μm [BSi] and % >51 μm [POC] at z_{PAR} are important factors in POC transfer in the upper mesopelagic zone.

The relationships between the attenuation of >51 μm [POC] and >51 μm [BSi] and particle size fractionation may arise from a more fundamental feature shared by both high-[BSi] and large-particle stations of the Great Calcite Belt: diatom-rich phytoplankton communities. Indeed, we also observe a strong correlation between >51 μm [BSi] and % >51 μm [POC] at z_{PAR} (p<<0.001, r^2= 0.65; not shown). This is a consistent feature across diatom-rich populations, which produce large, BSi-rich organic aggregates that sink rapidly out of the euphotic zone (Michaels and Silver, 1988;

Sarah Rosengard 5/21/15 3:42 PM
Deleted: -rich

Sarah Rosengard 5/20/15 5:50 PM
Deleted: dominated

Buesseler, 1998; Thomalla et al. 2006). Indeed, euphotic zone diatom abundances enumerated with a FlowCam® are significantly correlated with >51 µm [BSi] at zPAR at corresponding stations in GB1 and GB2 (see supplement; Fig. S2a). Thus, characteristics describing ecosystem structure may underlie the correlation between BSi export and POC export in the Great Calcite Belt (Francois et al. 2002; Thomalla et al., 2008; Henson et al., 2012a; Henson et al., 2012b).

However, ecosystem composition does not directly explain why larger particles exported into the mesopelagic zone are remineralized more vigorously hundreds of meters below (Fig. 10b). It is paradoxical that the same large particles that sink quickly out of the euphotic zone would then remineralize faster, as well. This association between attenuation coefficient and particle size suggests that these particles sink more slowly than expected in the mesopelagic zone given their size (for example, as a result of high porosity and low excess density), and/or that they are subject to faster remineralization compared to regions with more POC in the small size fraction. Francois et al. (2002) noted a negative relationship between bathypelagic transfer efficiency and opal flux, and attributed this to increased lability in large diatom aggregates. Though we do not observe any negative correlation between upper mesopelagic transfer efficiency (T_{100}) and BSi fluxes at z_{PAR}, we suggest that potentially higher degradability of POC produced by diatom-rich communities may similarly explain the relationship between particle size and >51 µm [POC] attenuation in the upper mesopelagic zone.

Sarah Rosengard 5/20/15 5:50 PM
Deleted: dominated

The view of POC quality as a driving factor behind POC transfer argues for a deterministic role of euphotic zone community structure in POC transfer below the euphotic zone. It supports the conventional perspective that diatom-dominated communities are strong exporters of large, sinking POC particles out of the euphotic zone (Buesseler, 1998; Guidi et al., 2009), but also adds to the growing view that these communities have poor transfer efficiency and high attenuation through the mesopelagic zone (Francois et al., 2002; Guidi et al., 2009; Henson et al., 2012b; Henson et al., 2012a).

For instance, station GB1-85, with over half of [POC] in the >51 µm size class fraction in the euphotic zone (Fig. 6c; Table 3), has a low >51 µm [PIC]:[BSi] ratio of 0.035 at z_{PAR} (indicated in log-scale in Figs. 10a and 10b), which indicates relatively high

Sarah Rosengard 5/20/15 5:44 PM
Deleted: a community dominated by

diatom populations producing large BSi-rich aggregates (Figs. 2, S2, S3). Station GB1-85 exhibits a high export efficiency (Ez-ratio= 0.38, within the upper quartile of the data set), and the highest >51 µm [POC] and export fluxes at z_{PAR} (Figs. 5b, 7b, 8a; Table 3). Notably, >51 µm [POC] values in the lower mesopelagic zone are also the highest at GB1-85, despite attenuating greatly below zPAR (attenuation coefficient = 1.7) (Figs. 3, 8b, 8c; Table 2). But, because of high attenuation, proportionally less organic carbon transfers to the deep sea at GB1-85. The same diatom-rich communities that vigorously export POC ultimately may not sequester as much organic carbon in the deep ocean or draw down as much atmospheric CO_2 (Kwon et al., 2009) as would be expected considering the magnitude of export alone.

In contrast to a model diatom community like station GB1-85, station GB1-25 is BSi-deplete, with a >51 µm [PIC]:[BSi] ratio of 1.4 at z_{PAR} (indicated in log-scale in Fig. 10a), indicating relatively more coccolithophores in the community (Figs. S2, S3). With proportionally less POC in the >51 µm size-fraction (only 3.2%) (Figs. 6c, 10b; Table 3), >51 µm [POC] at GB1-25 attenuates little through the mesopelagic zone (attenuation coefficient = 0.4, the lowest of the data set) such that a third of the >51 µm [POC] at z_{PAR} remains at 1000m, compared to only 1.4% at station GB1-85 (Fig. 3). At GB1-25, export efficiency is very low (Ez-ratio=0.04), suggesting that the particles exiting the euphotic zone here have been recycled vigorously in the euphotic zone prior to export, which may explain their low >51 µm [POC] and high proportion in the <51 µm size-fraction at z_{PAR}. In the mesopelagic zone, these particles are not very reactive and thus remineralize very little, perhaps sequestering a higher proportion of the CO_2 fixed in the euphotic zone.

Several other stations with proportionally more small particles and weaker >51 µm [POC] attenuation in the mesopelagic zone exhibit higher >51 µm [PIC] than >51 µm [BSi] at z_{PAR} (labeled in the lower left quadrant of Fig. 10b), suggesting that export regimes characterized by high relative abundance of coccolithophores consistently transfer less reactive POC to the mesopelagic zone. Artificial roller tank experiments have demonstrated that coccolithophore cultures can produce smaller, more compact aggregates than diatom cultures, partly because of smaller cell sizes (Iversen and Ploug, 2010). However, smaller size does not necessarily mean slower sinking velocities (e.g., McDonnell and Buesseler, 2010). Iversen and Ploug (2010) showed that the higher

Sarah Rosengard 5/20/15 5:44 PM
Deleted: s

Sarah Rosengard 5/15/15 11:12 AM
Deleted: also have a short length scale of remineralization, and

Sarah Rosengard 5/19/15 1:58 PM
Deleted: the

Sarah Rosengard 5/20/15 5:46 PM
Deleted: 4

Sarah Rosengard 5/20/15 5:48 PM
Deleted: the dominance

Sarah Rosengard 5/20/15 5:47 PM
Deleted: of

Sarah Rosengard 5/20/15 5:48 PM
Deleted: over

Sarah Rosengard 5/20/15 5:48 PM
Deleted: diatoms

Sarah Rosengard 5/20/15 5:50 PM
Deleted: dominated

Sarah Rosengard 5/20/15 5:50 PM
Deleted: over diatoms

excess density of these small aggregates generated faster sinking speeds than similarly sized pure diatom aggregates. Another roller tank study that compared aggregate formation by calcifying versus non-calcifying coccolithophores observed that aggregates formed from calcifying coccolithophores were smaller but faster sinking (Engel et al., 2009). In regions like the Great Calcite Belt, dense coccolithophore populations may similarly export small, highly degraded and compact particles out of the euphotic zone. As a result, these communities would efficiently transfer POC towards the base of the mesopelagic zone, even if the magnitude of exported POC is not as high as in diatom-rich regions (Thomalla et al., 2008; Guidi et al., 2009; Henson et al., 2012b). This may explain why higher PIC export fluxes are associated with higher transfer efficiencies but not higher POC flux at z_{PAR} (Fig. 9), and also why the ballast association between PIC and POC fluxes appears only at greater depths (Francois et al., 2002; Klaas and Archer, 2002).

Attenuation coefficients for >51 µm [POC] across diatom-rich regions exhibit a great spread (standard deviation= 0.47), ranging from 0.47 to 1.88. Not all diatom-rich stations (i.e., >51 µm [PIC]:[BSi]<1 at z_{PAR}) have proportionally larger particles or higher b-values (e.g., stations GB1-70, GB1-77 and GB2-87; Fig. 10b). In contrast, attenuation coefficients across coccolithophore-rich regions (i.e., >51 µm [PIC]:[BSi] ≥ 1 at z_{PAR}) exhibit a lower standard deviation (0.31) and a smaller range, 0.35 to 1.12. The greater variance in attenuation across BSi-rich regions may result from sampling the diatom populations at different seasons of the bloom cycle (Lam et al., 2011), and implies that there may be less seasonality in POC transfer to depth in coccolithophore-rich regions. Indeed, massive diatom export events with high transfer efficiency through the mesopelagic zone have been observed (Martin et al., 2011; Smetacek et al. 2012), so there are clearly conditions that can lead to efficient mesopelagic POC transfer from diatom blooms.

It is worth noting that >51 µm [PIC]:[BSi] ratios did increase with depth at most stations of the Great Calcite Belt, as might be expected because BSi is undersaturated in seawater. The possibility that BSi dissolves faster than PIC in particles sinking through the mesopelagic zone would complicate the connections we draw between diatom-rich communities in the euphotic zone and the attenuation of >51 µm [POC]. But, there are no

Sarah Rosengard 5/15/15 11:12 AM
Deleted: the remineralization length scale of calcareous assemblages is likely to be longer than regions dominated by diatom assemblages. T

Sarah Rosengard 5/20/15 5:50 PM
Deleted: dominated

Sarah Rosengard 5/20/15 5:51 PM
Deleted: dominated

Sarah Rosengard 5/20/15 5:52 PM
Deleted: ,

Sarah Rosengard 5/20/15 5:52 PM
Deleted: such that n

Sarah Rosengard 5/20/15 5:52 PM
Deleted: dominated by diatoms

Sarah Rosengard 5/20/15 5:51 PM
Deleted: dominated

Sarah Rosengard 5/20/15 5:53 PM
Deleted: dominated

Sarah Rosengard 5/20/15 5:53 PM
Deleted: dominated

associations between the magnitude of [PIC]:[BSi] increase and >51 μm [BSi] at z_{PAR}, >51 μm [PIC] at z_{PAR} or >51 μm [POC] attenuation with depth, suggesting that the issue of differential dissolution should not significantly impact our earlier interpretations. In the future, directly evaluating the degradability of sinking POC using organic characterization techniques (e.g., ramped pyrolysis or biomarker isolation) (e.g., Wakeham et al., 2002; Rosenheim et al., 2008; Rosenheim and Galy, 2012; Rosenheim et al., 2013) would greatly improve our ability to track the transformation of POC produced by different ecosystem assemblages across the Great Calcite Belt.

5 Conclusion

In summary, we argue here that phytoplankton assemblages play a fundamental role (Francois et al., 2002; Thomalla et al., 2008; Henson et al., 2012b; Henson et al., 2012a) in determining the fate of POC export through the Great Calcite Belt region, the effect of which sometimes, but not always, appears as a mineral ballast mechanism in the euphotic zone (Lam et al., 2011; Henson et al., 2012a; Lima et al., 2013). Though shallow BSi export fluxes were strongly correlated with POC export fluxes, they are also associated with diatom communities that produce larger particles that attenuate more quickly through the mesopelagic zone, such that proportionally less POC reaches the lower mesopelagic zone, and proportionally more is returned to the water column as remineralized carbon (dissolved inorganic and organic carbon).

Author contributions:

S.Z. Rosengard, the primary author, participated in the GB2 field work, sample analysis in lab and writing. P.J. Lam contributed to field work during GB2, and participated in both data interpretation and editing the manuscript. W.M. Balch, supplied the primary productivity and light profile data included here, and provided valuable feedback during writing. M.E. Auro and S. Pike participated in field work and sample analysis during and after GB1. D. Drapeau and B. Bowler contributed to field work during both GB1 and GB2, as well as sample analysis, particularly with respect to primary productivity and light profile data.

Acknowledgements:

Many thanks to Ken Buesseler for discussions and lending us field equipment; Dan Ohnemus, Angela Warner, Michael Brown, Rebecca Fowler, and Marina Van der Eb for help at sea; and Laura Lubelczyk, Paul Henderson, and Scott Birdwhistell for analytical work/assistance. This work was funded by NSF OCE-0960880 to P.J. Lam, and NSF OCE-0961660, NASA NNX11A072G and NNX11AL93G to W.M. Balch.

References

Abramson, L., Lee, C., Liu, Z. F., Wakeham, S. G., and Szlosek, J.: Exchange between suspended and sinking particles in the northwest Mediterranean as inferred from the organic composition of in situ pump and sediment trap samples, Limnology and Oceanography, 55, 725-739, 2010.

Armstrong, R. A., Lee, C., Hedges, J. I., Honjo, S., and Wakeham, S. G.: A new, mechanistic model for organic carbon fluxes in the ocean based on the quantitative association of POC with ballast minerals, Deep-Sea Research Part Ii-Topical Studies in Oceanography, 49, 219-236, 2002.

Balch, W. M., Drapeau, D., and Fritz, J.: Monsoonal forcing of calcification in the Arabian Sea, Deep-Sea Research II, 47, 1301-1337, 2000.

Balch, W. M., Drapeau, D. T., Bowler, B. C., Lyczkowski, E. R., Lubelczyk, L. C., Painter, S. C., and Poulton, A. J.: Surface biological, chemical, and optical properties of the Patagonian Shelf coccolithophore bloom, the brightest waters of the Great Calcite Belt, Limnology and Oceanography, 59, 1715-1732, 2014.

Balch, W. M., Drapeau, D. T., Bowler, B. C., Lyczskowski, E., Booth, E. S., and Alley, D.: The contribution of coccolithophores to the optical and inorganic carbon budgets during the Southern Ocean Gas Exchange Experiment: New evidence in support of the Great Calcite Belt hypothesis, J. Geophys. Res., 116, C00F06, 2011a.

Balch, W. M., Poulton, A. J., Drapeau, D. T., Bowler, B. C., Windecker, L. A., and Booth, E. S.: Zonal and meridional patterns of phytoplankton biomass and carbon fixation in the Equatorial Pacific Ocean, between 110°W and 140°W, Limnology and Oceanography, 59, 1715-1732, 2011b.

1208 Belkin, I. M. and Gordon, A. L.: Southern Ocean fronts from the Greenwich meridian to
1209 Tasmania, Journal of Geophysical Research: Oceans (1978–2012), 101, 3675-
1210 3696, 1996.
1211
1212 Bishop, J. K. B., Lam, P. J., and Wood, T. J.: Getting good particles: accurate sampling
1213 of particles by large volume in-situ filtration, Limnology and Oceanography
1214 Methods, 10, 681-710, 2012.
1215
1216 Brzezinski, M. A. and Nelson, D. M.: Seasonal changes in the silicon cycle within a Gulf
1217 Stream warm-core ring, Deep Sea Research Part A. Oceanographic Research
1218 Papers, 36, 1009-1030, 1989.
1219
1220 Buesseler, K., Lamborg, C. H., Cai, P., Escoube, R., Johnson, R., Pike, S., Masque, P.,
1221 McGillicuddy, D., and Verdeny, E.: Particle fluxes associated with mesoscale
1222 eddies in the Sargasso Sea, Deep-Sea Research II, 55, 1426-1444, 2008.
1223
1224 Buesseler, K. O.: The decoupling of production and particulate export in the surface
1225 ocean, Global Biogeochemical Cycles, 12, 297-310, 1998.
1226
1227 Buesseler, K. O., Ball, L., Andrews, J., Cochran, J. K., Hirschberg, D. J., Bacon, M. P.,
1228 Fleer, A., and Brzezinski, M.: Upper ocean export of particulate organic carbon
1229 and biogenic silica in the Southern Ocean along 170 degrees W, Deep-Sea
1230 Research Part II-Topical Studies in Oceanography, 48, 4275-4297, 2001.
1231
1232 Buesseler, K. O., Barber, R. T., Dickson, M. L., Hiscock, M. R., Moore, J. K., and
1233 Sambrotto, R.: The effect of marginal ice-edge dynamics on production and
1234 export in the Southern Ocean along 170 degrees W, Deep-Sea Research Part Ii-
1235 Topical Studies in Oceanography, 50, 579-603, 2003.
1236
1237 Buesseler, K. O., Benitez-Nelson, C. R., Moran, S. B., Burd, A., Charette, M., Cochran,

Sarah Rosengard 5/21/15 9:43 AM
Deleted: i

J. K., Coppola, L., Fisher, N. S., Fowler, S. W., and Gardner, W. D.: An assessment of particulate organic carbon to thorium-234 ratios in the ocean and their impact on the application of ^{234}Th as a POC flux proxy, Marine Chemistry, 100, 2006.

Buesseler, K. O. and Boyd, P.: Shedding light on processes that control particle export and flux attenuation in the twilight zone of the open ocean, Limnol, Oceanogr, 54, 1210-1232, 2009.

Buesseler, K. O., Lamborg, C. H., Boyd, P. W., Lam, P. J., Trull, T. W., Bidigare, R. R., Bishop, J. K. B., Casciotti, K. L., Dehairs, F., Elskens, M., Honda, M., Karl, D. M., Siegel, D. A., Silver, M. W., Steinberg, D. K., Valdes, J., Van Mooy, B., and Wilson, S.: Revisiting carbon flux through the ocean's twilight zone, Science, 316, 567-570, 2007.

Buesseler, K. O., Pike, S., Maiti, K., Lamborg, C. H., Siegel, D. A., and Trull, T. W.: Thorium-234 as a tracer of spatial, temporal and vertical variability in particle flux in the North Pacific, Deep Sea Research Part I: Oceanographic Research Papers, 56, 1143-1167, 2009.

Cochran, J. K., Buesseler, K. O., Bacon, M. P., Wang, H. W., Hirschberg, D. J., Ball, L., Andrews, J., Crossin, G., and Fleer, A.: Short-lived thorium isotopes (Th-234, Th-228) as indicators of POC export and particle cycling in the Ross Sea, Southern Ocean, Deep-Sea Research Part Ii-Topical Studies in Oceanography, 47, 3451-3490, 2000.

Coppola, L., Roy-Barman, M., Mulsow, S., Povinec, P., and Jeandel, C.: Low particulate organic carbon export in the frontal zone of the Southern Ocean (Indian sector) revealed by Th-234, Deep-Sea Research Part I-Oceanographic Research Papers, 52, 51-68, 2005.

De La Rocha, C. L., Nowald, N., and Passow, U.: Interactions between diatom aggregates, minerals, particulate organic carbon, and dissolved organic matter: Further implications for the ballast hypothesis, Global Biogeochemical Cycles, 22, 2008.

Engel, A., Szlosek, J., Abramson, L., Liu, Z., and Lee, C.: Investigating the effect of ballasting by $CaCO_3$ in Emiliania huxleyi: I. Formation, settling velocities and physical properties of aggregates, Deep Sea Research Part II: Topical Studies in Oceanography, 56, 1396-1407, 2009.

Fabry, V. J. and Balch, W. M.: Direct measurements of calcification rates in planktonic organisms., U. Riebeseil, V.J. Fabry, L. Hansson and J.-P. Gattuso (Editors), Guide to Best Practices in Ocean Acidification Research and Data Reporting. European Project on Ocean Acidification (EPOCA), Bremerhaven, Germany, 2010. 185-196, 2010.

Francois, R., Honjo, S., Krishfield, R., and Manganini, S.: Factors controlling the flux of organic carbon to the bathypelagic zone of the ocean, Global Biogeochemical Cycles, 16, 1087, doi:10.1029/2001GB001722, 2002.

Friedrich, J. and van der Loeff, M. M. R.: A two-tracer (Po-210-Th-234) approach to distinguish organic carbon and biogenic silica export flux in the Antarctic Circumpolar Current, Deep-Sea Research Part I-Oceanographic Research Papers, 49, 101-120, 2002.

Giering, S. L. C., Sanders, R., Lampitt, R. S., Anderson, T. R., Tamburini, C., Boutrif, M., Zubkov, M. V., Marsay, C. M., Henson, S. A., Saw, K., Cook, K., and Mayor, D. J.: Reconciliation of the carbon budget in the ocean/'s twilight zone, Nature, 507, 480-483, 2014.

Glover, D. M., Jenkins, W. J., and Doney, S. C.: Modeling methods for marine science.,

Cambridge University Press, New York, 2011.

Guidi, L., Stemmann, L., Jackson, G. A., Ibanez, F., Claustre, H., Legendre, L., Picheral, M., and Gorsky, G.: Effects of phytoplankton community on production, size and export of large aggregates: A world-ocean analysis, Limnology and Oceanography, 54, 1951-1963, 2009.

Hedges, J. I. and Oades, J. M.: Comparative organic geochemistries of soils and marine sediments, Organic Geochemistry, 27, 319-361, 1997.

Henson, S., Lampitt, R., and Johns, D.: Variability in phytoplankton community structure in response to the North Atlantic Oscillation and implications for organic carbon flux, Limnology and Oceanography, 57, 1591, 2012a.

Henson, S. A., Sanders, R., and Madsen, E.: Global patterns in efficiency of particulate organic carbon export and transfer to the deep ocean, Global Biogeochem. Cycles, 26, GB1028, 2012b.

Henson, S. A., Sanders, R., Madsen, E., Morris, P. J., Le Moigne, F., and Quartly, G. D.: A reduced estimate of the strength of the ocean's biological carbon pump, Geophys. Res. Lett., 38, L04606, 2011.

Henson, S. A., Yool, A., and Sanders, R.: Variability in efficiency of particulate organic carbon export: A model study, Global Biogeochem. Cycles, 29, GB004965, 2015.

Honjo, S., Francois, R., Manganini, S., Dymond, J., and Collier, R.: Particle fluxes to the interior of the Southern Ocean in the Western Pacific sector along 170 degrees W, Deep-Sea Research Part Ii-Topical Studies in Oceanography, 47, 3521-3548, 2000.

Iversen, M. H. and Ploug, H.: Ballast minerals and the sinking carbon flux in the ocean:

Sarah Rosengard 5/21/15 12:31 PM
Deleted: 2011.

Sarah Rosengard 5/21/15 9:46 AM
Formatted: Indent: First line: 0.5"

carbon-specific respiration rates and sinking velocity of marine snow aggregates, Biogeosciences, 7, 2613-2624, 2010.

Jacquet, S. H. M., Lam, P. J., Trull, T., and Dehairs, F.: Carbon export production in the subantarctic zone and polar front zone south of Tasmania, Deep Sea Research Part II: Topical Studies in Oceanography, 58, 2277-2292, 2011.

Klaas, C. and Archer, D. E.: Association of sinking organic matter with various types of mineral ballast in the deep sea: Implications for the rain ratio, Global Biogeochemical Cycles, 16, 1116-1129, 2002.

Kwon, E. Y., Primeau, F., and Sarmiento, J. L.: The impact of remineralization depth on the air-sea carbon balance, Nature Geoscience, 2, 630-635, 2009.

Lam, P. J. and Bishop, J. K. B.: High biomass, low export regimes in the Southern Ocean, Deep Sea Research Part II: Topical Studies in Oceanography, 54, 601-638, 2007.

Lam, P. J., Doney, S. C., and Bishop, J. K. B.: The dynamic ocean biological pump: Insights from a global compilation of particulate organic carbon, $CaCO_3$, and opal concentration profiles from the mesopelagic, Global Biogeochem. Cycles, 25, GB3009, 2011.

Lam, P. J., Ohnemus, D. C., and Auro, M. E.: Size-fractionated major particle composition and concentrations from the US GEOTRACES north Atlantic zonal transect, Deep Sea Research Part II: Topical Studies in Oceanography, 2014. 2014.

Le Moigne, F., Henson, S., Sanders, R., and Madsen, E.: Global database of surface ocean particulate organic carbon export fluxes diagnosed from the 234 Th technique, Earth System Science Data Discussions, 6, 163-187, 2013.

Le Moigne, F. A. C., Pabortsava, K., Marcinko, C. L. J., Martin, P., and Sanders, R. J.: Where is mineral ballast important for surface export of particulate organic carbon in the ocean?, Geophysical Research Letters, doi: 10.1002/2014GL061678, 2014. 2014GL061678, 2014.

Le Moigne, F. A. C., Sanders, R. J., Villa-Alfageme, M., Martin, A. P., Pabortsava, K., Planquette, H., Morris, P. J., and Thomalla, S. J.: On the proportion of ballast versus non-ballast associated carbon export in the surface ocean, Geophys. Res. Lett., 39, L15610, 2012.

Lima, I. D., Lam, P. J., and Doney, S. C.: Dynamics of particulate organic carbon flux in a global ocean model, Biogeosciences Discuss., 10, 14715-14767, 2013.

Lomas, M. W., Steinberg, D. K., Dickey, T., Carlson, C. A., Nelson, N. B., Condon, R. H., and Bates, N. R.: Increased ocean carbon export in the Sargasso Sea linked to climate variability is countered by its enhanced mesopelagic attenuation, Biogeosciences, 7, 57-70, 2010.

Maiti, K., Benitez-Nelson, C. R., Rii, Y., and Bidigare, R.: The influence of a mature cyclonic eddy on particle export in the lee of Hawaii, Deep Sea Research Part II: Topical Studies in Oceanography, 55, 1445-1560, 2012.

Martin, J. H., Knauer, G. A., Karl, D. M., and Broenkow, W. W.: Vertex - Carbon Cycling in the Northeast Pacific, Deep-Sea Research Part a-Oceanographic Research Papers, 34, 267-285, 1987.

Martin, P., Lampitt, R. S., Jane Perry, M., Sanders, R., Lee, C., and D'Asaro, E.: Export and mesopelagic particle flux during a North Atlantic spring diatom bloom, Deep Sea Research Part I: Oceanographic Research Papers, 58, 338-349, 2011.

Sarah Rosengard 5/18/15 3:33 PM
Deleted: and Buesseler, K. O.

Sarah Rosengard 5/18/15 3:34 PM
Deleted: Insights into particle formati ... [1]

Sarah Rosengard 5/18/15 3:34 PM
Formatted: Indent: Left: 0"

Sarah Rosengard 5/18/15 3:34 PM
Deleted: , Thoruim-234

Sarah Rosengard 5/18/15 3:34 PM
Deleted: Geophysical Research Letters

Sarah Rosengard 5/18/15 3:34 PM
Deleted: 37

Sarah Rosengard 5/18/15 3:33 PM
Deleted: 2010

McCave, I. N.: Vertical flux of particles in the ocean, Deep Sea Research, 22, 491-502, 1975.

McDonnell, A. M. P. and Buesseler, K. O.: Variability in the average sinking velocities of marine particles, Limnology and Oceanography, 55, 2085-2096, 2010.

Michaels, A. F. and Silver, M. W.: Primary production, sinking fluxes and the microbial food web, Deep Sea Research Part A. Oceanographic Research Papers, 35, 473-490, 1988.

Morris, P. J., Sanders, R., Turnewitsch, R., and Thomalla, S.: Th-234-derived particulate organic carbon export from an island-induced phytoplankton bloom in the Southern Ocean, Deep-Sea Research Part Ii-Topical Studies in Oceanography, 54, 2208-2232, 2007.

Owens, S., Buesseler, K., and Sims, K.: Re-evaluating the ^{238}U-salinity relationship in seawater: Implications for the ^{238}U–^{234}Th disequilibrium method, Marine Chemistry, 127, 31-39, 2011.

Paasche, E. and Brubak, S.: Enhanced calcification in the coccolithophorid *Emiliania huxleyi* (Haptophyceae) under phosphorus limitation, Phycologia, 33, 324-330, 1994.

Passow, U. and De la Rocha, C. L.: Accumulation of mineral ballast on organic aggregates, Global Biogeochemical Cycles, 20, 2006.

Pike, S. M., Buesseler, K. O., Andrews, J., and Savoye, N.: Quantification of Th-234 recovery in small volume sea water samples by inductively coupled plasma-mass spectrometry, Journal of Radioanalytical and Nuclear Chemistry, 263, 355-360, 2005.

1433 Pilson, M. E. Q.: An Introduction to the Chemistry of the Sea, Cambridge University
1434 Press, New York, 2012. 2012.
1435
1436 Planchon, F., Cavagna, A.-J., Cardinal, D., André, L., and Dehairs, F.: Late summer
1437 particulate organic carbon export and twilight zone remineralisation in the
1438 Atlantic sector of the Southern Ocean, Biogeosciences, 10, 803-820, 2013.
1439
1440 Resplandy, L., Martin, A. P., Le Moigne, F., Martin, P., Aquilina, A., Mémery, L., Lévy,
1441 M., and Sanders, R.: How does dynamical spatial variability impact ^{234}Th-derived
1442 estimates of organic export?, Deep Sea Research Part I: Oceanographic Research
1443 Papers, 68, 24-45, 2012.
1444
1445 Riley, J. S., Sanders, R., Marsay, C., Le Moigne, F. A. C., Achterberg, E. P., and Poulton,
1446 A. J.: The relative contribution of fast and slow sinking particles to ocean carbon
1447 export, Global Biogeochem. Cycles, 26, GB1026, 2012.
1448
1449 Rodriguez y Baena, A. M., Boudjenoun, R., Fowler, S. W., Miquel, J. C., Masqué, P.,
1450 Sanchez-Cabeza, J.-A., and Warnau, M.: ^{234}Th-based carbon export during an ice-
1451 edge bloom: Sea-ice algae as a likely bias in data interpretation, Earth and
1452 Planetary Science Letters, 269, 596-604, 2008.
1453
1454 Rosenheim, B. E., Day, M. B., Domack, E., Schrum, H., Benthien, A., and Hayes, J. M.:
1455 Antarctic sediment chronology by programmed-temperature pyrolysis:
1456 Methodology and data treatment, Geochemistry, Geophysics, Geosystems, 9,
1457 2008.
1458
1459 Rosenheim, B. E. and Galy, V.: Direct measurement of riverine particulate organic
1460 carbon age structure, Geophysical Research Letters, 39, 2012.
1461
1462 Rosenheim, B. E., Roe, K. M., Roberts, B. J., Kolker, A. S., Allison, M. A., and

Johannesson, K. H.: River discharge influences on particulate organic carbon age structure in the Mississippi/Atchafalaya River System, Global Biogeochemical Cycles, 27, 154-166, 2013.

Rutgers van der Loeff, M. M., Cai, P. H., Stimac, I., Bracher, A., Middag, R., Klunder, M. B., and van Heuven, S. M.: ^{234}Th in surface waters: Distribution of particle export flux across the Antarctic Circumpolar Current and in the Weddell Sea during the GEOTRACES expedition ZERO and DRAKE, Deep Sea Research Part II: Topical Studies in Oceanography, 58, 2749-2766, 2011.

Rutgers Van Der Loeff, M. M., Friedrich, J., and Bathmann, U. V.: Carbon export during the Spring Bloom at the Antarctic Polar Front, determined with the natural tracer ^{234}Th, Deep Sea Research Part II: Topical Studies in Oceanography, 44, 457-478, 1997.

Rutgers van der Loeff, M. M., Sarin, M. M., Baskaran, M., Benitez-Nelson, C., Buesseler, K. O., Charette, M., Dai, M., Gustafsson, r., Masque, P., Morris, P. J., Orlandini, K., Rodriguez y Baena, A., Savoye, N., Schmidt, S., Turnewitsch, R., Vˆge, I., and Waples, J. T.: A review of present techniques and methodological advances in analyzing ^{234}Th in aquatic systems, Marine Chemistry, 100, 190-212, 2006.

Sanders, R., Morris, P. J., Poulton, A. J., Stinchcombe, M. C., Charalampopoulou, A., Lucas, M. I., and Thomalla, S. J.: Does a ballast effect occur in the surface ocean?, Geophysical Research Letters, 37, L08602, 2010.

Santschi, P., Murray, J. W., Baskaran, M., Benitez-Nelson, C. R., Guo, L., Hung, C.-C., Lamborg, C., Moran, S. B., Passow, U., and Roy-Barman, M.: Thorium speciation in seawater, Marine Chemistry, 100, 250-268, 2006.

Sarmiento, J. L., Dunne, J., Gnanadesikan, A., Key, R. M., Matsumoto, K., and Slater,

1494 R.: A new estimate of the $CaCO_3$ to organic carbon export ratio, Global
1495 Biogeochemical Cycles, 16, 2002.
1496
1497 Sarmiento, J. L., Gruber, N., Brzezinski, M. A., and Dunne, J. P.: High-latitude controls
1498 of thermocline nutrients and low latitude biological productivity, Nature, 427, 56-
1499 60, 2004.
1500
1501 Savoye, N., Benitez-Nelson, C., Burd, A. B., Cochran, J. K., Charette, M., Buesseler, K.
1502 O., Jackson, G. A., Roy-Barman, M., Schmidt, S., and Elskens, M.: Th-234
1503 sorption and export models in the water column: A review, Marine Chemistry,
1504 100, 234-249, 2006.
1505
1506 Savoye, N., Trull, T. W., Jacquet, S. H. M., Navez, J., and Dehairs, F.: ^{234}Th-based
1507 export fluxes during a natural iron fertilization experiment in the Southern Ocean
1508 (KEOPS), Deep Sea Research Part II: Topical Studies in Oceanography, 55, 841-
1509 855, 2008.
1510
1511 Shimmield, G. B., Ritchie, G. D., and Fileman, T. W.: The Impact of Marginal Ice-Zone
1512 Processes on the Distribution of Pb-210, Po-210 and Th-234 and Implications for
1513 New Production in the Bellingshausen Sea, Antarctica, Deep-Sea Research Part
1514 Ii-Topical Studies in Oceanography, 42, 1313-1335, 1995.
1515
1516 Smetacek, V., Klaas, C., Strass, V. H., Assmy, P., Montresor, M., Cisewski, B., Savoye,
1517 N., Webb, A., d'Odivio, F., Arrieta, J. M., Bathmann, U., Bellerby, R., Berg, G.
1518 M., Croot, P., Gonzalez, S., Henjes, J., Herndl, G. J., Hoffmann, L. J., Leach, H.,
1519 Losch, M., Mills, M. M., Neill, C., Peeken, I., Röttgers, R., Sachs, O., Sauter, E.,
1520 Schmidt, M. M., Schwarz, J., Terbrüggen, A., and Wolf-Gladrow, D.: Deep
1521 carbon export from a Southern Ocean iron-fertilized diatom bloom, Nature, 487,
1522 7407, 313-319, 2012.
1523
1524 Sokolov, S. and Rintoul, S. R.: Circumpolar structure and distribution of the Antarctic

1525 Circumpolar Current fronts: 1. Mean circumpolar paths, Journal of Geophysical
1526 Research: Oceans (1978–2012), 114, 2009.
1527 Steinberg, D. K., Van Mooy, B. A. S., Buesseler, K. O., Boyd, P. W., Kobari, T., and
1528 Karl, D. M.: Bacterial vs. zooplankton control of sinking particle flux in the
1529 ocean's twilight zone, Limnology and Oceanography, 53, 1327-1338, 2008.
1530
1531 Strickland, J. D. and Parsons, T. R.: A practical handbook of seawater analysis, Fisheries
1532 Research Board of Canada Ottawa, 1968.
1533
1534 Thomalla, S., Turnewitsch, R., Lucas, M., and Poulton, A.: Particulate organic carbon
1535 export from the North and South Atlantic gyres: The ^{234}Th/^{238}U disequilibrium
1536 approach, Deep Sea Research Part II: Topical Studies in Oceanography, 53, 1629-
1537 1648, 2006.
1538
1539 Thomalla, S. J., Poulton, A. J., Sanders, R., Turnewitsch, R., Holligan, P. M., and Lucas,
1540 M. I.: Variable export fluxes and efficiencies for calcite, opal, and organic carbon
1541 in the Atlantic Ocean: A ballast effect in action?, Global Biogeochem. Cycles, 22,
1542 GB1010, 2008.
1543
1544 Trull, T. W., Bray, S. G., Buesseler, K. O., Lamborg, C. H., Manganini, S., Moy, C., and
1545 Valdes, J.: In situ measurement of mesopelagic particle sinking rates and the
1546 control of carbon transfer to the ocean interior during the Vertical Flux in the
1547 Global Ocean (VERTIGO) voyages in the North Pacific, Deep-Sea Research Part
1548 Ii-Topical Studies in Oceanography, 55, 1684-1695, 2008.
1549
1550 Volk, T. and Hoffert, M. I.: Ocean carbon pumps: Analysis of relative strengths and
1551 efficiencies in ocean-driven atmospheric CO_2 changes, Geophysical Monographs,
1552 32, 99-110, 1985.
1553
1554 Wakeham, S. G., Peterson, M. L., Hedges, J. I., and Lee, C.: Lipid biomarker fluxes in

the Arabian Sea, with a comparison to the equatorial Pacific Ocean, Deep-Sea Research Part Ii-Topical Studies in Oceanography, 49, 2265-2301, 2002.

Wilson, J. D., Barker, S., and Ridgwell, A.: Assessment of the spatial variability in particulate organic matter and mineral sinking fluxes in the ocean interior: Implications for the ballast hypothesis, Global Biogeochemical Cycles, 26, GB4011, 2012.

Wilson, S. E., Steinberg, D. K., and Buesseler, K. O.: Changes in fecal pellet characteristics with depth as indicators of zooplankton repackaging of particles in the mesopelagic zone of the subtropical and subarctic North Pacific Ocean, Deep-Sea Research Part Ii-Topical Studies in Oceanography, 55, 1636-1647, 2008.

Zhou, K., Nodder, S., Dai, M., and Hall, J.: Insignificant enhancement of export flux in the highly productive subtropical front, east of New Zealand: a high resolution study of particle export fluxes based on ^{234}Th: ^{238}U disequilibria, Biogeosciences, 9, 973-992, 2012.

Table 1. Locations and times of sampling of total ^{234}Th and size-fractionated particles on cruises GB1 and GB2. Two export depths are indicated: z_{PAR} (depth of 0.3% of surface photosynthetically available radiation) and $z_{Th/U}$ (depth where ^{234}Th and ^{238}U activities return to secular equilibrium below surface deficits).

Sarah Rosengard 5/20/15 3:01 PM
Deleted: active

Cruise	Station	Date	Lat.	Long.	z_{PAR}	$z_{Th/U}$
-	-	*dd-mm-yy*	*deg. N*	*deg. E*	*m*	*m*
GB1	6	14 Jan 2011	-51.79	-56.11	79	130
GB1	16	17 Jan 2011	-46.26	-59.83	62	141
GB1	25	20 Jan 2011	-45.67	-48.95	62	115
GB1	32	22 Jan 2011	-40.95	-46.00	69	171
GB1	38	24 Jan 2011	-36.52	-43.38	121	121
GB1	46	26 Jan 2011	-42.21	-41.21	63	100
GB1	59	29 Jan 2011	-51.36	-37.85	60	95
GB1	70	1 Feb 2011	-59.25	-33.15	100	100
GB1	77	3 Feb 2011	-57.28	-25.98	98	100
GB1	85	5 Feb 2011	-53.65	-17.75	73	140
GB1	92	7 Feb 2011	-50.40	-10.80	59	100
GB1	101	9 Feb 2011	-46.31	-3.21	81	140
GB1	109	11 Feb 2011	-42.63	3.34	76	130
GB1	117	13 Feb 2011	-38.97	9.49	62	110
GB2	5	21 Feb 2012	-36.94	39.60	78	90
GB2	27	26 Feb 2012	-45.82	51.05	105	105
GB2	36	28 Feb 2012	-46.84	58.25	90	90
GB2	43	1 Mar 2012	-47.53	64.01	108	125
GB2	53	3 Mar 2012	-49.30	71.32	81	100
GB2	63	5 Mar 2012	-54.40	74.54	109	130
GB2	73	7 Mar 2012	-59.71	77.73	93	75
GB2	87	10 Mar 2012	-54.23	88.22	107	100
GB2	93	11 Mar 2012	-49.81	94.13	113	130
GB2	100	14 Mar 2012	-44.62	100.50	113	90
GB2	106	16 Mar 2012	-40.10	105.34	102	95
GB2	112	17 Mar 2012	-40.26	109.63	76	105
GB2	119	20 Mar 2012	-42.08	113.40	92	90

Table 2. POC fluxes, concentrations, and attenuation of >51 μm [POC] in the mesopelagic zone. Attenuation coefficient is the exponent from significant power law fits to >51 μm [POC]. z_{PAR}+100m is 100 m below z_{PAR}, as defined in the Table 1 caption. Transfer efficiency is POC flux at z_{PAR}+100m divided by POC flux at z_{PAR}. Deep >51 μm [POC] was measured at 1000 m and 800 m for GB1 and GB2, respectively. POC flux errors are propagated from ^{234}Th flux, and POC:^{234}Th errors.

Cruise	Station	Depth	>51 μm [POC] Attenuation Coefficient	^{234}Th Flux at z_{PAR} + 100m	POC:Th at z_{PAR} + 100m	POC Flux at z_{PAR} + 100m	Transfer Efficiency	>51 μm [POC] (≥800m)
-	-	*m*	*unitless*	*dpm m^{-2}d^{-1}*	*μmol dpm^{-1}*	*mmol m^{-2}d^{-1}*	*unitless*	*μM*
GB1	6	179	0.8	3,319± 128[c]	1.7	5.7 ± 0.31	1.00	0.030
GB1	16	162	1.1	2,567 ± 116[c]	2.4	6.1 ± 0.30	1.04	No data
GB1	25	162	0.4	1,074 ± 125	2.5	2.7 ± 0.37	1.76	0.013
GB1	32	169	0.9	1,581 ± 186	1.3	2.0 ± 0.25	0.86	0.006
GB1	38	221	No fit	911 ± 206	1.6	1.5 ± 0.35	0.70	0.026
GB1	46	163	1.0	1,937 ± 146	1.6	3.1 ± 0.27	0.4	0.009
GB1	59	160	0.6	2,582 ± 126[c]	3.7	9.5 ± 0.56	1.29	0.014
GB1	70	200	0.6	1,414 ± 248	3.5	5.0 ± 0.90	0.90	0.024
GB1	77	198	0.5	1,903 ± 162	2.1	4.0 ± 0.41	0.44	0.012
GB1	85	173	1.7[a]	2,076 ± 207	3.9	8.1 ± 0.83	0.41	0.035
GB1	92	159	1.1	1,339 ± 170	3.7	4.9 ± 0.64	0.61	0.019
GB1	101	181	0.8	1,774 ± 135	1.7	3.0 ± 0.24	0.83	0.019
GB1	109	176	1.0	1,719 ± 97	1.1	1.9 ± 0.13	0.87	0.006
GB1	117	162	1.1	1,258 ± 86	1.2	1.5 ± 0.13	0.87	0.005
GB2	5	178	0.5	1,402 ± 3,706[c]	1.1	1.5 ± 6.1	0.5	No data
GB2	27	205	No fit	2,063 ± 205	1.2	2.5 ± 0.30	0.71	No data
GB2	36	190	1.5	1,077 ± 194	0.9	0.93 ± 0.18	0.48	0.011
GB2	43	208	1.9	1,247 ± 200	2.2	2.7 ± 0.45	0.54	0.005
GB2	53	181	No fit	1,013 ± 220	2.0	2.0 ± 0.45	0.49	No data
GB2	63	209	1.8	1,292 ± 262	1.7	2.1 ± 0.46	0.31	0.014
GB2	73	193	1.5	807 ± 189	1.9	1.6 ± 0.37	0.48	0.008
GB2	87	207	0.7	1,213 ± 196	1.6	1.9 ± 0.34	0.60	0.013
GB2	93	213	*2.3*[b]	469 ± 249	1.6	0.77 ± 0.42	0.53	0.001
GB2	100	213	0.8	1,132 ± 190	0.7	0.80 ± 0.15	0.52	0.014
GB2	106	202	0.9	1,405 ± 186	1.3	1.8 ± 0.26	1.63	0.017
GB2	112	176	1.3	270 ± 186	0.9	0.23 ± 0.21	0.24	0.007
GB2	119	192	No fit	756 ± 218	0.8	0.57 ± 0.17	0.20	0.013

[a] attenuation coefficient is 2.35 when only fitting > 51 μm [POC] measurements at depths <500 m (Fig. 3).
[b] outlier approximated by Chauvenet's Theorem (Glover, et al., 2011).

[c]values were estimated by linear interpolation of values at upper and lower depths around z_{PAR}+100m.
"no data": no measurements at these depths.
"no fit": power-law fit was not statistically significant (p>0.05).

Table 3. POC, biomineral, and ^{234}Th concentrations and fluxes at z_{PAR}. Ez- ratio is ^{234}Th-derived POC flux at z_{PAR} divided by integrated primary productivity. The % >51μm [POC] metric is the fraction of total [POC] in the >51 μm size fraction. POC and biomineral flux errors are propagated from ^{234}Th flux, and POC:^{234}Th errors.

Cruise	Station	z_{PAR}	^{234}Th Flux	>51um [POC]	>51um [Bsi]	>51um [PIC]	>51um Th activity	POC:Th	POC Flux	Bsi:Th	BSi Flux	PIC:Th	PIC Flux	Primary Productivity	Ez- Ratio	% >51 um [POC]
-	-	*m*	*dpm m^{-2}d^{-1}*	*uM*	*uM*	*uM*	*dpm L^{-1}*	*μmol dpm^{-1}*	*mmol m^{-2}d^{-1}*	*μmol dpm^{-1}*	*mmol m^{-2}d^{-1}*	*μmol dpm^{-1}*	*mmol m^{-2}d^{-1}*	*mmol m^{-2}d^{-1}*	*unitless*	*%*
GB1		6	79	2,437 ± 100	0.23 [b]	0.03 [a]	0.124 [a]	0.07 [a]	2.3 [a]	5.7 ± 0.26	0.4	0.9 ± 0.04	1.8	4.3 ± 0.20	42	0.14	8.8%
GB1		16	62	1,933 ± 71	0.38	0.08	0.390	0.12	3.0	5.9 ± 0.68	0.6	1.2 ± 0.14	3.1	6.1 ± 0.70	165	0.04	17.7%
GB1		25	62	862 ± 46 [a]	0.04	0.005 [a]	0.015 [a]	0.02	1.8	1.6 ± 0.11	0.2	0.2 ± 0.02	0.7	0.6 ± 0.04	35	0.04	3.2%
GB1		32	69	1,304 ± 116	0.07	0.01	0.027	0.04	1.8	2.3 ± 0.21	0.3	0.3 ± 0.03	0.7	0.9 ± 0.08	11	0.21	3.9%
GB1		38	121	809 ± 126	0.04	0.003	0.017	0.01	2.7	2.2 ± 0.35	0.2	0.2 ± 0.03	1.2	0.9 ± 0.15	21	0.10	8.4%
GB1		46	63	2,123 ± 69	0.23	0.005	0.059	0.06	4.1	8.8 ± 0.38	0.1	0.2 ± 0.02	1.1	2.2 ± 0.10	13	0.67	5.3%
GB1		59	60	1,844 ± 102	0.09	0.10	0.072	0.02	4.0	7.3 ± 0.52	4.6	8.6 ± 0.53	3.4	6.2 ± 0.39	26	0.28	5.3%
GB1		70	100	1,280 ± 94	0.11	0.06 [a]	0.001 [a]	0.02	4.3	5.5 ±	3.5 [a]	4.5 ±	0.1 [a]	0.1 ±	10	0.53	10.6%

									0.44		0.35		0.09			
GB1	77	98	1,485 ± 105	0.03	0.03	0.002	0.01	6.0	9.0 ±	5.6	8.3 ±	0.4	0.7 ±	57	0.16	3.6%
									1.3		0.98		0.23			
GB1	85	73	1,858 ± 94	2.50	3.44	0.124	0.23	10.8	20 ±	14.9	28 ±	0.5	1.0 ±	53	0.38	52.0%
									1.1		1.5		0.05			
GB1	92	59	1,639 ± 77	0.40	0.46	0.020	0.08	4.9	8.0 ±	5.6	9.3 ±	0.2	0.4 ±	26	0.31	11.3%
									0.40		0.46		0.02			
GB1	101	81	1,763 ± 82	0.19	0.05	0.013	0.09	2.0	3.6 ±	0.5	0.9 ±	0.1	0.2 ±	22	0.17	12.5%
									0.18		0.04		0.01			
GB1	109	76	1,524 ± 76	0.19 [a]	0.05[a]	0.027 [a]	0.14 [a]	1.4	2.1 ±	0.4	0.6 ±	0.2	0.3 ±	14	0.16	21.0%
									0.11		0.03		0.02			
GB1	117	62	1,177 ± 50	0.21	0.02	0.032	0.15	1.4	1.7 ±	0.1	0.2 ±	0.2	0.3 ±	18	0.09	6.6%
									0.07		0.01		0.01			
GB2	5	78	1,889 ± 5207	0.08[b]	0.01[a]	0.048 [a]	0.05 [a]	1.6	3.0 ±	0.2	0.4 ±	1.0	1.9 ±	8.2	0.37	7.6%
									8.8		1.2		5.2			
GB2	27	105	1,869 ± 160	0.08[a]	0.10[a]	0.060 [a]	0.04 [a]	1.9	3.5 ±	2.2	4.0 ±	1.3	2.5 ±	8.0	0.44	6.7%
									0.32		0.35		0.22			
GB2	36	90	988 ± 89	0.43	0.28	0.074	0.22	2.0	2.0 ±	1.3	1.3 ±	0.3	0.3 ±	12	0.16	15.6%
									0.18		0.12		0.03			
GB2	43	108	1,221 ± 153	0.74 [a]	0.62 [a]	0.041 [a]	0.18 [a]	4.1	5.0 ±	3.4	4.2 ±	0.2	0.3 ±	12	0.43	37.8%
									0.63		0.53		0.04			
GB2	53	81	1058 ± 100 [a]	0.54 [a]	0.80 [a]	0.081 [a]	0.14 [a]	3.9	4.1 ±	5.7	6.1 ±	0.6	0.6 ±	16	0.25	22.5%
									0.40		0.59		0.07			
GB2	63	109	1,229 ± 138	0.71 [a]	1.04 [a]	0.028 [a]	0.13 [a]	5.6 [a]	6.9 ±	8.1	9.9 ±	0.2	0.3 ±	9.0	0.77	33.2%
									0.78		1.1		0.03			
GB2	73	93	977 ± 108	0.21 [b]	1.13 [a]	0.014 [a]	0.20 [a]	3.3 [a]	3.2 ±	5.6	5.4 ±	0.1	0.1 ±	8.8	0.36	17.6%
									0.36		0.60		0.01			

GB2	87	107	1,299 ± 115	0.06 [b]	0.30 [a]	0.041 [a]	0.06 [a]	2.5 [a]	3.2 ± 0.40	4.7	6.1 ± 0.55	0.6	0.8 ± 0.14	11	0.29	3.4%
GB2	93	113	1,142 ± 137	0.07 [a]	0.01 [a]	0.023 [a]	0.05 [a]	1.3	1.5 ± 0.25	0.2	0.3 ± 0.06	0.4	0.5 ± 0.14	12	0.12	4.3%
GB2	100	113	1,112 ± 130	0.08	0.02	0.006	0.06	1.4	1.5 ± 0.19	0.3	0.3 ± 0.04	0.1	0.1 ± 0.02	14	0.11	12.8%
GB2	106	102	1394 ± 82[a]	0.09 [b]	0.04 [a]	0.024 [a]	0.12 [a]	0.8	1.1 ± 0.86	0.3 [a]	0.4 ± 0.02	0.2	0.3 ± 0.02	22	0.05	12.2%
GB2	112	76	717 ± 97	0.22 [b]	0.17 [a]	0.087 [a]	0.36 [a]	1.4 [a]	1.0 ± 0.13	0.5	0.3 ± 0.05	0.2	0.2 ± 0.02	no data	no data	13.3%
GB2	119	92	1,223 ± 124	0.51 [a]	0.12 [a]	0.048 [a]	0.22 [a]	2.3	2.8 ± 0.29	0.5	0.7 ± 0.07	0.2	0.3 ± 0.03	17	0.17	21.5%

[a] values at z_{PAR} estimated by linear interpolation of values at upper and lower depths around z_{PAR}.
[b] >51 µm [POC] values interpolated by significant power-law fits (Fig. 3).
"no data": not enough depths were sampled and analyzed to interpolate at z_{PAR}.

1601 Table 4. Mean ± standard deviations of ^{234}Th fluxes, POC:^{234}Th, BSi: ^{234}Th, PIC: ^{234}Th, POC fluxes, and biomineral fluxes at z_{PAR},
1602 divided by three latitude zones. 45 °S marks the approximate latitude of the Subantarctic front, while 52 °S marks the approximate
1603 latitude of the Polar front (Belkin and Gordon, 1996; Sokolov and Rintoul, 2009).
1604

Lat. zone	**^{234}Th Flux at z_{PAR}**	**POC:Th at z_{PAR}**	**POC Flux at z_{PAR}**	**BSi:Th at z_{PAR}**	**BSi Flux at z_{PAR}**	**PIC:Th at z_{PAR}**	**PIC Flux at z_{PAR}**	**# stn**
°S	*dpm $m^{-2}d^{-1}$*	*µmol dpm^{-1}*	*mmol $m^{-2}d^{-1}$*	*µmol dpm^{-1}*	*mmol $m^{-2}d^{-1}$*	*µmol dpm^{-1}*	*mmol $m^{-2}d^{-1}$*	-
36 - 45	1.3 ± 0.44	1.9 ± 0.9	2.7 ± 2.3	0.3 ± 0.1	0.33 ± 0.17	0.5 ± 0.4	0.73 ± 0.76	10
45 – 52	1.5 ± 0.50	2.8 ±1.2	4.4 ± 2.2	2.3 ± 2.2	3.4 ± 3.3	1.1 ± 1.2	2.0 ± 2.4	11
52 - >60	1.4 ± 0.30	5.4 ± 3.0	8.0 ± 6.3	7.1 ± 4.1	10 ± 8.7	0.3 ± 0.2	0.49 ± 0.4	6

1605 Figure 1. Cruise tracks across the Atlantic (cruise GB1) and Indian (cruise GB2) sectors
1606 of the Great Calcite Belt showing sea surface temperature along the two transects. Station
1607 numbers where only ^{234}Th and size-fractionated particles were sampled are indicated by
1608 crosses. The two horizontal dashed lines at 45 °S and 52 °S represent the approximate
1609 locations of the Subantarctic and Polar fronts, respectively (Belkin and Gordon, 1996;
1610 Sokolov and Rintoul, 2009).

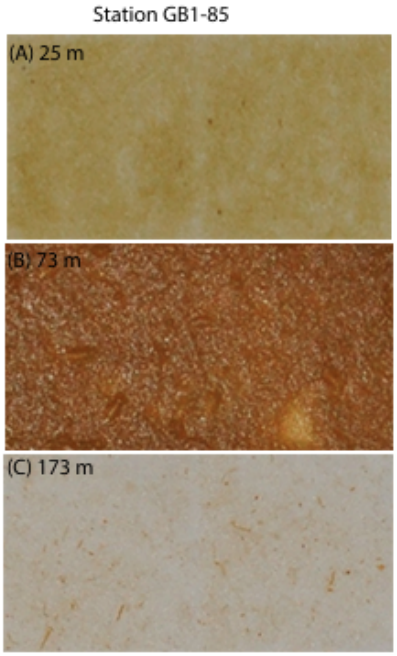

1611

1612 Figure 2. Digital images of >51 µm filters from station GB1-85 (refer to Fig. 1 for station
1613 location). >51 µm particles are from (a) 25m in the euphotic zone, (b) 73m, which
1614 corresponds to z_{PAR}, as defined in Table 1, and (c) at 173m, below both metrics of export
1615 depth, z_{PAR} and $z_{Th/U}$ (Table 1). >51 µm particles in the euphotic zone appear as dense
1616 sheets of intact cells packed onto the filters (a, b) and as more sparsely arranged
1617 cylindrical fecal pellets on filters collected below z_{PAR} (c).

Sarah Rosengard 5/19/15 11:27 AM
Deleted: in the euphotic zone

1618

1619 Figure 3. Significant power law fits of >51 µm [POC] below z_{PAR}, according to Eq. (1).
1620 Only the 22 significant fits are shown as lines. Three stations are highlighted to show the
1621 range in >51 µm [POC] attenuation across GB1 and GB2 profiles (symbols represent

measurements): GB1-85 had the highest POC concentration through the water column and an attenuation coefficient of 1.7; GB1-25 had the lowest attenuation coefficient (0.4); GB2-43 had the highest attenuation coefficient (1.9) (Table 2). Fitting GB1-85 >51 μm [POC] measurements between z_{PAR} and 500 m yields a higher attenuation coefficient of 2.35. Refer to Fig. 1 for station locations.

Figure 4. Total ^{234}Th and ^{238}U activity profiles measured at 14 stations of GB1 and 13 stations of GB2 (note different x-axis for station GB2-5) (Table S1). Error bars for ^{234}Th activity are propagated errors. ^{238}U is calculated from salinity. All ^{234}Th activity profiles exhibit a deficit relative to ^{238}U activity at the surface, and mostly return to equilibrium with ^{234}U within error at depth of $z_{Th/U}$ (Table 1). Refer to Fig. 1 for station locations.

Figure 5. Distribution of ^{234}Th flux and ^{234}Th-derived POC flux at 27 stations along GB1 and GB2 (circle area scales with flux magnitude). (a) ^{234}Th fluxes at z_{PAR} range from 717 dpm m^{-2} d^{-1} to 2,437 dpm m^{-2} d^{-1} at stations GB2-112 and GB1-6, respectively. (b) POC fluxes at z_{PAR} range from 0.97 mmol m^{-2} d^{-1} to 20 mmol m^{-2} d^{-1}at stations GB2-112 and GB1-85, respectively. (c) POC fluxes at $z_{Th/U}$ range from 0.57 to 12 mmol m^{-2} d^{-1} at stations GB2-112 and GB1-85, respectively (Table S2). (d) POC fluxes at 100m below z_{PAR} range from 0.23 to 9.5 mmol m^{-2} d^{-1} at stations GB2-112 and GB1-59, respectively. A few station numbers discussed in the text are indicated. Red outlines distinguish stations where fluxes are greater at the specified depth than at z_{PAR}. The two horizontal dashed lines at 45 °S and 52 °S represent the approximate locations of the Subantarctic and Polar fronts, respectively (Belkin and Gordon, 1996; Sokolov and Rintoul, 2009). Refer to Fig. 1 for other station locations. z_{PAR} and $z_{Th/U}$ are defined as in Table 1.

Figure 6. Distribution of BSi flux, PIC flux, and % >51 μm [POC], the percent of total [POC] in the >51 μm size class, at z_{PAR} (Table 1) along GB1 and GB2 (circle area scales with magnitude). (a) BSi fluxes range from 0.17 mmol m^{-2} d^{-1} to 28 mmol m^{-2} d^{-1} at stations GB1-46 and GB1-85, respectively. (b) PIC fluxes range from 0.067 to 6.2 mmol m^{-2} d^{-1}at stations GB2-73 and GB2-59, respectively. (c) The proportion of [POC] in the >51 μm size-fraction at z_{PAR} ranges from 3.3% to 52% at stations GB1-25 and GB1-85,

1654 respectively. A few station numbers discussed in the text are indicated. The two
1655 horizontal dashed lines at 45 °S and 52 °S represent the approximate locations of the
1656 Subantarctic and Polar fronts, respectively (Belkin and Gordon, 1996; Sokolov and
1657 Rintoul, 2009). Refer to Fig. 1 for other station locations.
1658
1659 Figure 7. Distribution of primary productivity, export efficiency, and transfer efficiency
1660 along GB1 and GB2 (circle area scales with magnitude). (a) Primary productivity
1661 integrated through the euphotic zone ranges from 8.0 to 165 mmol m^{-2} d^{-1} at stations
1662 GB2-27 and GB1-16, respectively. (b) Export efficiency (Ez-ratio) at z_{PAR} (Table 1),
1663 which is the ratio of ^{234}Th-derived POC flux at z_{PAR} to primary productivity integrated to
1664 z_{PAR}, ranges from 0.04 to 0.77 at stations GB1-16 and GB2-63, respectively. (c) Transfer
1665 efficiency at z_{PAR}, which is the ratio of POC flux 100 m below z_{PAR} to POC flux at z_{PAR},
1666 ranges from 0.20 to 1.8 at stations GB1-119 and GB1-25, respectively. A few station
1667 numbers discussed in the text are indicated. The two horizontal dashed lines at 45 °S and
1668 52 °S represent the approximate locations of the Subantarctic and Polar fronts,
1669 respectively (Belkin and Gordon, 1996; Sokolov and Rintoul, 2009). Refer to Fig. 1 for
1670 other station locations.
1671
1672 Figure 8. Distribution and vertical attenuation coefficient of >51 µm [POC] (circle area
1673 scales with magnitude). (a) >51 µm POC concentrations at z_{PAR} (Table 1) range from
1674 0.03 µM to 2.5 µM at stations GB1-77 and GB1-85, respectively. (b) >51 µm [POC] at
1675 the deepest pump depth in the lower mesopelagic zone (800 m-1000 m). Concentrations
1676 range from 0.001 µM to 0.035 µM at stations GB2-93 and GB1-85, respectively. (c)
1677 Attenuation coefficient from significant power-law fits of 22 >51 µm [POC] profiles,
1678 excluding GB2-93 (see Sect. 4.4). A few station numbers discussed in the text are
1679 indicated. The two horizontal dashed lines at 45 °S and 52 °S represent the approximate
1680 locations of the Subantarctic and Polar fronts, respectively (Belkin and Gordon, 1996;
1681 Sokolov and Rintoul, 2009). Refer to Fig. 1 for other station locations.
1682
1683 Figure 9. ^{234}Th-derived POC flux as a function of (a) PIC flux and (b) BSi flux at z_{PAR}.
1684 POC flux transfer efficiency between z_{PAR} and z_{PAR}+100 m (T_{100}, defined in Sect. 4.4) as

a function of (c) PIC flux and (d) BSi flux at z_{PAR}. Significant linear relationships are plotted as a solid blue line. T_{100} values at GB1-25 and GB2-106 were excluded from all correlations (Sect. 4.4). Colorbar indicates longitude of stations— GB1 and GB2 stations are in cool and warm colors, respectively. Refer to Fig. 1 for more specific station locations.

Figure 10. Attenuation coefficient as a function of (a) >51 µm [BSi] at z_{PAR} and (b) the proportion of [POC] in the >51 µm size-fraction at z_{PAR}. The open circle indicates where GB1-85 would plot with a higher attenuation coefficient of 2.35, derived from fitting >51 µm [POC] at depths between z_{PAR} and 500 m. Significant linear relationships using the lower and higher attenuation coefficient values for GB1-85 are shown as solid and dashed lines, respectively; p and r^2 values are provided for the solid lines. The colorbar is the natural logarithm of the ratio of >51 µm PIC:BSi at z_{PAR}. We interpret all warm colors >0 to indicate stations with a high relative abundance of coccolithophores, and all cool values <0 to indicate stations with a high relative abundance of diatoms (Figs. S2, S3). A few station numbers discussed in the text are indicated. Refer to Fig. 1 for station locations.

Sarah Rosengard 5/20/15 5:54 PM
Deleted: -dominated

Sarah Rosengard 5/20/15 5:54 PM
Deleted: stations

Sarah Rosengard 5/20/15 5:54 PM
Deleted: -dominated stations

Supplement Contents

This supplement contains, in the following order:

Table S1. ^{234}Th activity and flux profiles estimated at 27 stations along cruises GB1 and GB2. Fluxes were estimated by measuring total seawater ^{234}Th activity deficits relative to total seawater ^{238}U activity, as described in Sect. 2.4. ^{234}Th flux errors are propagated from ^{234}Th activity errors.

Cruise	Station	Depth	^{234}Th Activity	^{234}Th Activity Error	^{238}U Activity	^{234}Th Flux	^{234}Th Flux Error
-	-	*m*	*dpm L^{-1}*	*dpm L^{-1}*	*dpm L^{-1}*	*dpm m^{-2} d^{-1}*	*dpm m^{-2} d^{-1}*
GB1	6	13.6	1.04	0.02	2.36	681	27
GB1	6	22.3	1.28	0.05	2.36	924	31
GB1	6	29.2	1.12	0.03	2.36	1,243	34
GB1	6	40.2	1.23	0.03	2.36	1,503	37
GB1	6	45.2	1.29	0.06	2.36	1,702	39
GB1	6	53.1	1.53	0.04	2.36	2,096	48
GB1	6	78	1.86	0.12	2.36	2,437	100
GB1	6	100.6	1.90	0.05	2.36	2,684	106
GB1	6	115	2.08	0.10	2.36	2,804	116
GB1	6	130	2.15	0.05	2.36	2,911	121
GB1	6	150.3	2.09	0.07	2.36	3,182	145
GB1	6	200	2.04	0.18	2.37	3,419	195
GB1	16	11.1	0.99	0.02	2.35	548	20
GB1	16	17.07	1.10	0.02	2.35	762	22
GB1	16	23.04	0.94	0.02	2.35	1,107	25
GB1	16	34.2	1.61	0.04	2.35	1,311	30
GB1	16	42.2	1.61	0.05	2.36	1,611	42
GB1	16	62.3	1.97	0.05	2.36	1,933	71
GB1	16	100.17	2.06	0.05	2.36	2,277	105
GB1	16	140.8	2.18	0.06	2.37	2,487	139
GB1	16	180.1	2.24	0.08	2.37	2,636	178
GB1	16	220.5	2.21	0.21	2.37	2,819	308
GB1	16	260.7	2.37	0.13	2.37	2,810	394
GB1	16	340.3	2.16	0.08	2.37	3,040	409
GB1	25	10.3	1.70	0.05	2.45	283	26
GB1	25	16.1	1.95	0.06	2.45	380	30
GB1	25	23.8	1.91	0.03	2.45	525	34
GB1	25	34.5	2.14	0.05	2.47	611	38
GB1	25	41.7	2.07	0.07	2.47	773	51
GB1	25	80	2.42	0.03	2.48	941	74
GB1	25	115	2.46	0.04	2.45	937	91
GB1	25	140.5	2.38	0.05	2.43	975	103
GB1	25	165.2	2.32	0.07	2.44	1,074	125
GB1	25	200.2	2.44	0.04	2.42	1,029	177
GB1	25	300	2.36	0.03	2.38	1,051	195

GB1	32	12.15	1.96	0.08	2.48	229	41
GB1	32	18	1.96	0.06	2.48	327	44
GB1	32	25.25	2.00	0.07	2.49	475	51
GB1	32	39.2	2.02	0.10	2.49	614	61
GB1	32	46	2.05	0.19	2.49	808	104
GB1	32	69.67	1.83	0.04	2.47	1,304	116
GB1	32	100.2	2.33	0.03	2.48	1,435	127
GB1	32	130.5	2.38	0.03	2.47	1,520	141
GB1	32	171	2.41	0.09	2.46	1,581	186
GB1	32	210	2.43	0.03	2.46	1,612	198
GB1	32	251	2.29	0.11	2.45	1,818	250
GB1	32	300.8	2.52	0.03	2.44	1,761	253
GB1	38	20.4	2.36	0.08	2.52	127	72
GB1	38	32.2	2.17	0.03	2.52	247	74
GB1	38	44.2	2.20	0.04	2.52	418	83
GB1	38	69	2.28	0.10	2.53	550	102
GB1	38	81	2.27	0.08	2.54	638	107
GB1	38	92	2.34	0.03	2.53	743	113
GB1	38	121	2.43	0.05	2.51	809	126
GB1	38	150	2.41	0.09	2.50	886	151
GB1	38	175	2.57	0.05	2.50	811	168
GB1	38	220	2.43	0.06	2.50	911	206
GB1	38	280.2	2.47	0.05	2.48	938	247
GB1	38	350.7	2.74	0.08	2.48	678	265
GB1	46	10	1.40	0.02	2.43	395	20
GB1	46	16.8	1.47	0.03	2.43	573	23
GB1	46	23	1.54	0.03	2.43	813	28
GB1	46	35.7	1.41	0.02	2.42	1,090	32
GB1	46	42.03	1.37	0.02	2.42	1,338	34
GB1	46	52.1	1.36	0.03	2.42	1,652	38
GB1	46	62.7	1.74	0.07	2.42	2,123	69
GB1	46	100.4	2.44	0.03	2.41	2,089	102
GB1	46	150.4	2.51	0.05	2.40	1,937	146
GB1	46	200.4	2.46	0.05	2.40	1,850	174
GB1	46	250.2	2.37	0.11	2.39	1,874	283
GB1	46	325.3	2.53	0.12	2.38	1,712	314
GB1	59	10.4	1.46	0.03	2.34	335	21
GB1	59	16.1	1.43	0.06	2.34	493	25
GB1	59	22.5	1.64	0.21	2.34	673	61
GB1	59	34	1.61	0.12	2.34	857	69
GB1	59	40	1.50	0.03	2.34	1,013	70
GB1	59	47	1.49	0.05	2.34	1,256	73
GB1	59	60	1.49	0.09	2.34	1,844	102

GB1	59	95	2.12	0.05	2.35	2,108	128
GB1	59	140	2.05	0.06	2.36	2,509	159
GB1	59	185	2.24	0.09	2.37	2,673	202
GB1	59	225	2.16	0.05	2.37	3,113	244
GB1	59	325	2.34	0.04	2.40	3,189	262
GB1	70	17	1.86	0.06	2.36	314	47
GB1	70	27	1.85	0.06	2.36	460	52
GB1	70	37	1.76	0.05	2.36	721	61
GB1	70	57.5	1.81	0.06	2.36	967	69
GB1	70	68	1.90	0.05	2.37	1,119	72
GB1	70	80	2.05	0.05	2.37	1,266	80
GB1	70	100	2.36	0.06	2.38	1,280	94
GB1	70	125	2.29	0.18	2.38	1,361	190
GB1	70	160	2.35	0.06	2.39	1,412	208
GB1	70	200	2.40	0.09	2.40	1,414	248
GB1	70	250	2.45	0.09	2.40	1,342	286
GB1	70	300	2.27	0.06	2.41	1,439	292
GB1	77	17	1.71	0.06	2.35	399	45
GB1	77	26	1.68	0.05	2.35	573	49
GB1	77	35	1.84	0.05	2.35	794	57
GB1	77	56	1.79	0.06	2.35	1,047	66
GB1	77	66	1.86	0.06	2.35	1,197	70
GB1	77	77	1.97	0.06	2.36	1,391	79
GB1	77	101	2.25	0.08	2.37	1,485	105
GB1	77	130	2.30	0.06	2.39	1,561	122
GB1	77	160	2.31	0.06	2.39	1,630	139
GB1	77	190	2.16	0.05	2.40	1,903	162
GB1	77	240	2.40	0.07	2.40	1,917	213
GB1	77	300	2.40	0.13	2.41	1,922	243
GB1	85	12.6	1.30	0.05	2.35	476	32
GB1	85	19	1.55	0.07	2.35	629	35
GB1	85	26	1.41	0.06	2.35	925	43
GB1	85	41	1.52	0.07	2.35	1,197	52
GB1	85	49	1.76	0.07	2.35	1,340	56
GB1	85	58	1.91	0.07	2.35	1,493	63
GB1	85	73	1.86	0.08	2.35	1,858	94
GB1	85	110	2.17	0.09	2.36	2,034	133
GB1	85	140	2.34	0.09	2.36	2,059	168
GB1	85	180	2.36	0.09	2.37	2,076	207
GB1	85	220	2.46	0.09	2.38	1,931	273
GB1	85	300	2.60	0.10	2.39	1,683	300
GB1	92	10	1.68	0.07	2.34	239	32
GB1	92	15	1.61	0.07	2.34	365	35

GB1	92	22	1.54	0.07	2.34	571	41
GB1	92	33	1.78	0.04	2.34	709	43
GB1	92	39	1.65	0.05	2.34	837	45
GB1	92	46	1.59	0.04	2.34	1,053	48
GB1	92	59	1.59	0.06	2.34	1,639	77
GB1	92	100	2.65	0.07	2.35	1,332	117
GB1	92	130	2.28	0.06	2.36	1,396	134
GB1	92	160	2.41	0.09	2.36	1,339	170
GB1	92	200	2.42	0.06	2.37	1,248	232
GB1	92	302	2.29	0.06	2.38	1,391	259
GB1	101	13.6	1.57	0.04	2.36	405	33
GB1	101	22	1.46	0.04	2.36	611	35
GB1	101	29.5	1.58	0.05	2.36	867	42
GB1	101	45	1.61	0.05	2.36	1,133	49
GB1	101	54	1.74	0.06	2.37	1,296	52
GB1	101	63	1.89	0.06	2.37	1,484	61
GB1	101	81	1.96	0.07	2.37	1,763	82
GB1	101	110	2.24	0.07	2.38	1,878	107
GB1	101	140	2.43	0.05	2.37	1,826	122
GB1	101	171	2.43	0.05	2.37	1,774	135
GB1	101	200	2.44	0.05	2.37	1,641	184
GB1	101	300	2.20	0.04	2.37	1,883	205
GB1	109	11.1	1.58	0.03	2.39	318	23
GB1	109	16.2	1.69	0.04	2.39	445	25
GB1	109	23.7	1.62	0.04	2.39	672	31
GB1	109	36.5	1.77	0.04	2.40	854	35
GB1	109	44	1.76	0.04	2.48	1,158	44
GB1	109	66	2.03	0.04	2.40	1,326	53
GB1	109	76	1.99	0.04	2.40	1,524	61
GB1	109	100	2.17	0.04	2.39	1,648	71
GB1	109	115	2.19	0.04	2.40	1,737	76
GB1	109	130	2.43	0.05	2.40	1,722	83
GB1	109	150	2.40	0.05	2.40	1,719	94
GB1	109	175	2.40	0.05	2.40	1,719	97
GB1	117	10.5	1.80	0.04	2.43	243	24
GB1	117	16.3	1.69	0.03	2.43	377	26
GB1	117	23	1.99	0.04	2.43	484	30
GB1	117	33	1.77	0.04	2.41	659	34
GB1	117	42	1.95	0.04	2.41	758	37
GB1	117	48	1.86	0.04	2.42	918	41
GB1	117	62	1.87	0.04	2.43	1,177	50
GB1	117	80	2.08	0.04	2.44	1,346	58
GB1	117	95	2.31	0.05	2.44	1,404	65

GB1	117	110	2.46	0.05	2.44	1,394	71
GB1	117	125	2.61	0.05	2.43	1,290	82
GB1	117	150	2.52	0.05	2.43	1,258	86
GB2	5	20	1.37	6.03	2.47	948	5,206
GB2	5	40	1.70	0.08	2.47	1,403	5,206
GB2	5	61	1.84	0.07	2.47	1,768	5,206
GB2	5	71	1.89	0.15	2.48	2,015	5,206
GB2	5	80	2.18	0.07	2.47	1,889	5,207
GB2	5	90	2.56	0.07	2.47	1,862	5,207
GB2	5	100	2.52	0.08	2.48	1,850	5,207
GB2	5	111	2.54	0.08	2.47	1,832	5,207
GB2	5	120	2.44	0.09	2.47	1,849	5,207
GB2	5	150	2.50	0.07	2.48	1,821	5,208
GB2	5	201	2.82	0.14	2.47	1,058	5,218
GB2	5	300	2.71	0.09	2.46	695	5,220
GB2	27	20	1.70	0.04	2.34	554	53
GB2	27	40	1.56	0.04	2.34	1,114	69
GB2	27	70	1.68	0.06	2.34	1,637	92
GB2	27	85	1.53	0.24	2.34	2,047	155
GB2	27	95	1.97	0.05	2.34	1,828	159
GB2	27	105	2.20	0.06	2.35	1,869	160
GB2	27	115	2.21	0.08	2.35	1,910	162
GB2	27	125	2.28	0.06	2.35	1,931	164
GB2	27	135	2.27	0.05	2.35	1,972	168
GB2	27	160	2.18	0.06	2.35	2,130	181
GB2	27	200	2.41	0.06	2.36	2,063	205
GB2	27	250	2.69	0.08	2.36	1,826	216
GB2	36	20	1.83	0.04	2.34	434	55
GB2	36	40	1.86	0.06	2.34	639	65
GB2	36	50	1.82	0.08	2.34	824	73
GB2	36	65	1.91	0.05	2.34	981	77
GB2	36	75	2.19	0.08	2.35	1,035	84
GB2	36	90	2.48	0.06	2.35	988	89
GB2	36	100	2.29	0.08	2.35	1,034	117
GB2	36	125	2.04	0.07	2.35	1,372	148
GB2	36	150	2.23	0.06	2.35	1,161	169
GB2	36	175	2.42	0.06	2.35	1,110	178
GB2	36	200	2.39	0.05	2.36	1,077	194
GB2	36	250	2.58	0.07	2.36	923	202
GB2	43	20	1.89	0.04	2.33	383	55
GB2	43	40	1.90	0.08	2.33	632	76
GB2	43	60	1.93	0.08	2.33	896	99
GB2	43	85	2.06	0.07	2.34	1,034	108

GB2	43	95	2.03	0.05	2.34	1,147	111
GB2	43	110	2.17	0.24	2.34	1,221	153
GB2	43	125	2.25	0.05	2.34	1,258	156
GB2	43	140	2.25	0.10	2.34	1,308	169
GB2	43	165	2.45	0.06	2.34	1,233	177
GB2	43	190	2.35	0.06	2.35	1,230	186
GB2	43	220	2.33	0.07	2.35	1,247	200
GB2	43	250	2.68	0.09	2.36	1,108	205
GB2	53	20	1.87	0.08	2.34	407	80
GB2	53	40	1.88	0.14	2.34	668	117
GB2	53	60	1.99	0.05	2.34	915	126
GB2	53	90	1.98	0.05	2.34	1,120	132
GB2	53	100	2.27	0.08	2.34	1,139	134
GB2	53	110	2.45	0.06	2.34	1,109	136
GB2	53	120	2.40	0.06	2.34	1,056	151
GB2	53	170	2.38	0.11	2.35	1,013	220
GB2	53	210	2.52	0.06	2.35	827	237
GB2	53	250	2.30	0.06	2.36	860	241
GB2	63	20	1.88	0.09	2.34	394	88
GB2	63	40	1.94	0.08	2.34	625	102
GB2	63	60	1.95	0.08	2.34	848	115
GB2	63	80	1.92	0.05	2.34	1,089	121
GB2	63	100	2.12	0.13	2.34	1,187	135
GB2	63	110	2.20	0.08	2.34	1,229	138
GB2	63	120	2.25	0.10	2.34	1,285	151
GB2	63	130	2.31	0.10	2.34	1,316	174
GB2	63	150	2.37	0.09	2.35	1,267	191
GB2	63	175	2.38	0.09	2.35	1,248	204
GB2	63	200	2.32	0.14	2.36	1,292	262
GB2	63	250	2.50	0.09	2.37	1,198	272
GB2	73	20	1.80	0.06	2.35	433	63
GB2	73	35	1.79	0.06	2.35	675	71
GB2	73	50	1.94	0.09	2.35	823	79
GB2	73	60	1.96	0.07	2.35	966	85
GB2	73	75	2.30	0.11	2.37	997	99
GB2	73	90	2.43	0.09	2.38	977	108
GB2	73	105	2.63	0.07	2.39	822	120
GB2	73	120	2.58	0.12	2.39	677	156
GB2	73	135	2.43	0.06	2.40	794	168
GB2	73	160	2.34	0.06	2.40	853	184
GB2	73	200	2.48	0.06	2.40	807	189
GB2	87	20	1.93	0.07	2.35	354	71
GB2	87	40	1.92	0.05	2.35	599	81

GB2	87	60	1.75	0.06	2.35	939	91
GB2	87	80	1.89	0.07	2.35	1,134	98
GB2	87	90	1.88	0.05	2.35	1,268	100
GB2	87	100	2.28	0.08	2.35	1,290	103
GB2	87	110	2.33	0.13	2.35	1,299	115
GB2	87	125	2.35	0.08	2.36	1,302	121
GB2	87	140	2.36	0.08	2.36	1,297	136
GB2	87	170	2.32	0.08	2.36	1,336	159
GB2	87	200	2.48	0.09	2.37	1,213	196
GB2	87	250	2.55	0.08	2.38	1,088	208
GB2	93	20	1.95	0.07	2.36	352	71
GB2	93	40	2.04	0.09	2.36	554	96
GB2	93	65	2.14	0.08	2.36	710	116
GB2	93	90	1.95	0.08	2.36	944	127
GB2	93	105	2.01	0.08	2.36	1,071	132
GB2	93	115	2.17	0.10	2.37	1,142	137
GB2	93	130	2.57	0.09	2.39	1,061	144
GB2	93	145	2.44	0.08	2.39	1,033	152
GB2	93	165	2.42	0.08	2.39	1,003	170
GB2	93	180	2.40	0.09	2.39	992	213
GB2	93	200	2.82	0.09	2.39	469	249
GB2	93	250	2.61	0.09	2.38	309	259
GB2	100	20	1.89	0.05	2.42	464	58
GB2	100	40	1.90	0.07	2.42	764	75
GB2	100	60	2.06	0.07	2.42	922	83
GB2	100	70	1.80	0.05	2.42	1,101	85
GB2	100	80	2.27	0.08	2.43	1,145	89
GB2	100	90	2.33	0.08	2.43	1,174	94
GB2	100	100	2.66	0.28	2.43	1,110	124
GB2	100	110	2.43	0.08	2.43	1,112	130
GB2	100	130	2.30	0.09	2.43	1,205	151
GB2	100	160	2.48	0.09	2.43	1,157	182
GB2	100	200	2.47	0.08	2.43	1,132	190
GB2	106	20	1.87	0.05	2.47	603	68
GB2	106	50	1.77	0.05	2.47	1,005	79
GB2	106	60	1.83	0.06	2.47	1,189	82
GB2	106	70	2.09	0.08	2.48	1,301	86
GB2	106	80	2.17	0.08	2.48	1,413	92
GB2	106	95	2.45	0.09	2.48	1,426	107
GB2	106	115	2.62	0.09	2.48	1,335	126
GB2	106	140	2.50	0.06	2.48	1,320	138
GB2	106	165	2.36	0.06	2.48	1,423	154
GB2	106	200	2.49	0.07	2.47	1,405	186

GB2	106	250	2.64	0.17	2.46	1,274	226
GB2	112	10	2.11	0.08	2.42	136	40
GB2	112	20	2.39	0.09	2.42	149	54
GB2	112	35	2.29	0.08	2.42	199	65
GB2	112	45	1.91	0.07	2.43	347	69
GB2	112	55	1.80	0.07	2.42	526	73
GB2	112	65	2.25	0.09	2.42	589	82
GB2	112	80	2.20	0.08	2.43	717	97
GB2	112	105	2.47	0.09	2.43	682	126
GB2	112	135	2.66	0.09	2.42	466	160
GB2	112	170	2.63	0.09	2.42	270	186
GB2	112	200	2.69	0.10	2.42	-39	223
GB2	112	250	2.66	0.10	2.42	-211	237
GB2	119	10	1.73	0.19	2.42	347	96
GB2	119	25	1.73	0.05	2.42	644	101
GB2	119	40	1.77	0.06	2.42	923	106
GB2	119	55	2.00	0.07	2.42	1,072	110
GB2	119	65	2.16	0.07	2.43	1,147	113
GB2	119	74	2.21	0.07	2.43	1,226	117
GB2	119	90	2.43	0.08	2.43	1,223	124
GB2	119	105	2.32	0.08	2.42	1,280	135
GB2	119	130	2.60	0.08	2.43	1,127	158
GB2	119	165	2.69	0.09	2.42	853	189
GB2	119	200	2.50	0.08	2.42	756	218
GB2	119	250	2.75	0.09	2.42	516	231

Table S2. ^{234}Th and POC fluxes at $z_{Th/U}$, estimated at 27 stations along cruises GB1 and GB2. $z_{Th/U}$ is the depth where ^{234}Th and ^{238}U activities re-establish secular equilibrium. Calculations of POC flux from ^{234}Th fluxes are described in Sect. 2.4. POC flux errors are propagated from ^{234}Th flux, and POC:^{234}Th errors.

Cruise	Station	$z_{Th/U}$	^{234}Th Flux	^{234}Th Flux Error	>51µm POC:^{234}Th	POC Flux	POC Flux Error
-	-	*m*	*dpm m^{-2} d^{-1}*	*dpm m^{-2} d^{-1}*	*µmol dpm^{-1}*	*mmol m^{-2} d^{-1}*	*mmol m^{-2} d^{-1}*1
GB1	6	130	2,911	121	2.0	5.7	0.25
GB1	16	140.8	2,487	139	2.6	6.6	0.37
GB1	25	115	937	91	1.7	1.6	0.18
GB1	32	131	1,581	186	1.3	2.0	0.20
GB1	38	121	809	126	2.7	2.2	0.35
GB1	46	100	2,089	102	2.8	5.9	0.32
GB1	59	95	2,108	128	2.9	6.1	0.42
GB1	70	100	1,280	94	4.3	5.5	0.44
GB1	77	100	1,485	105	6.0	9.0	1.3
GB1	85	140	2,059	168	5.9	12	1.0
GB1	92	100	1,332	117	3.8	5.1	0.47
GB1	101	140	1,826	122	1.8	3.3	0.23
GB1	109	130	1,722	83	1.0	1.6	0.09
GB1	117	110	1,394	71	1.0	1.4	0.09
GB2	5	90	1,862	5,207	1.3	2.5	6.9
GB2	27	105	1,869	160	1.9	3.5	0.32
GB2	36	90	988	89	2.0	2.0	0.18
GB2	43	125	1,258	156	3.7	4.6	0.58
GB2	53	100	1,139	134	3.9	4.4	0.53
GB2	63	130	1,316	174	4.6	6.1	0.81
GB2	73	75	997	99	4.9	4.9	0.49
GB2	87	100	1,290	103	2.9	3.8	0.33
GB2	93	130	1,061	144	1.2	1.2	0.18
GB2	100	90	1,174	94	2.8	3.3	0.27
GB2	106	95	1,426	107	0.9	1.2	0.10
GB2	112	105	682	126	0.8	0.6	0.11
GB2	119	90	1,223	124	2.5	3.0	0.31

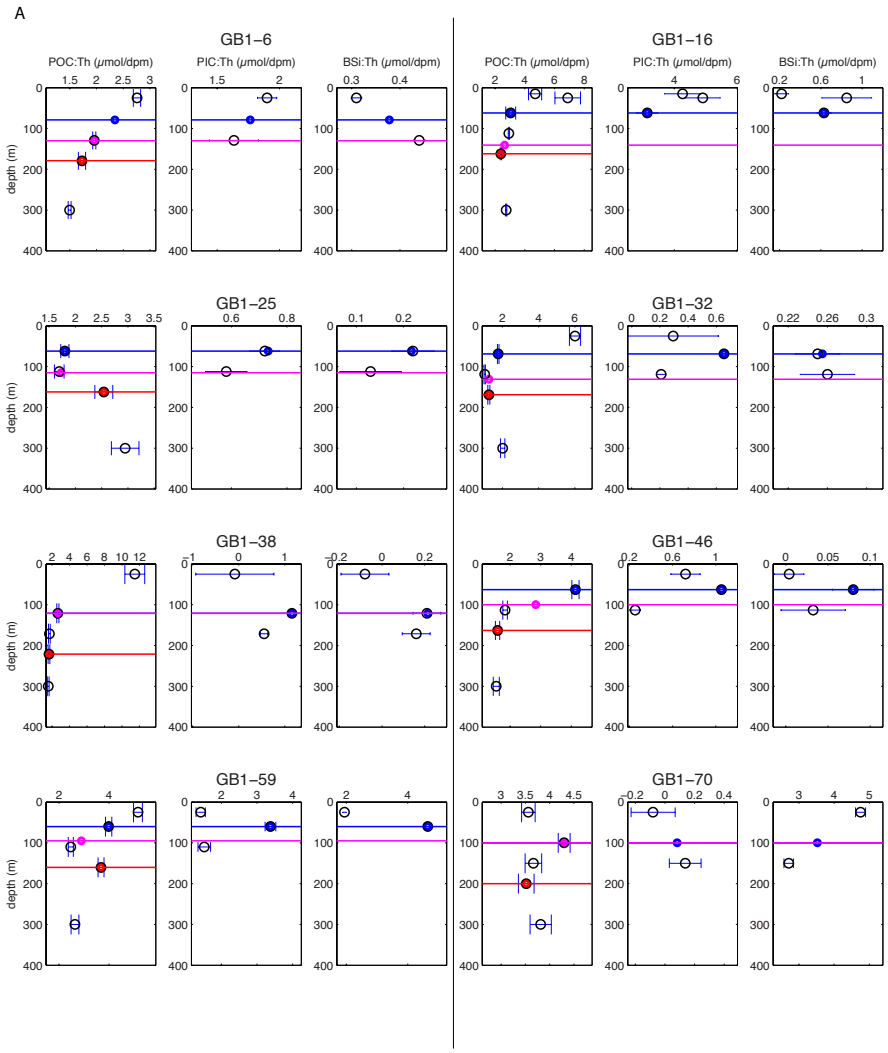
A
GB1−6
POC:Th (μmol/dpm)
PIC:Th (μmol/dpm)
BSi:Th (μmol/dpm)
GB1−16
GB1−25
GB1−32
GB1−38
GB1−46
GB1−59
GB1−70
depth (m)

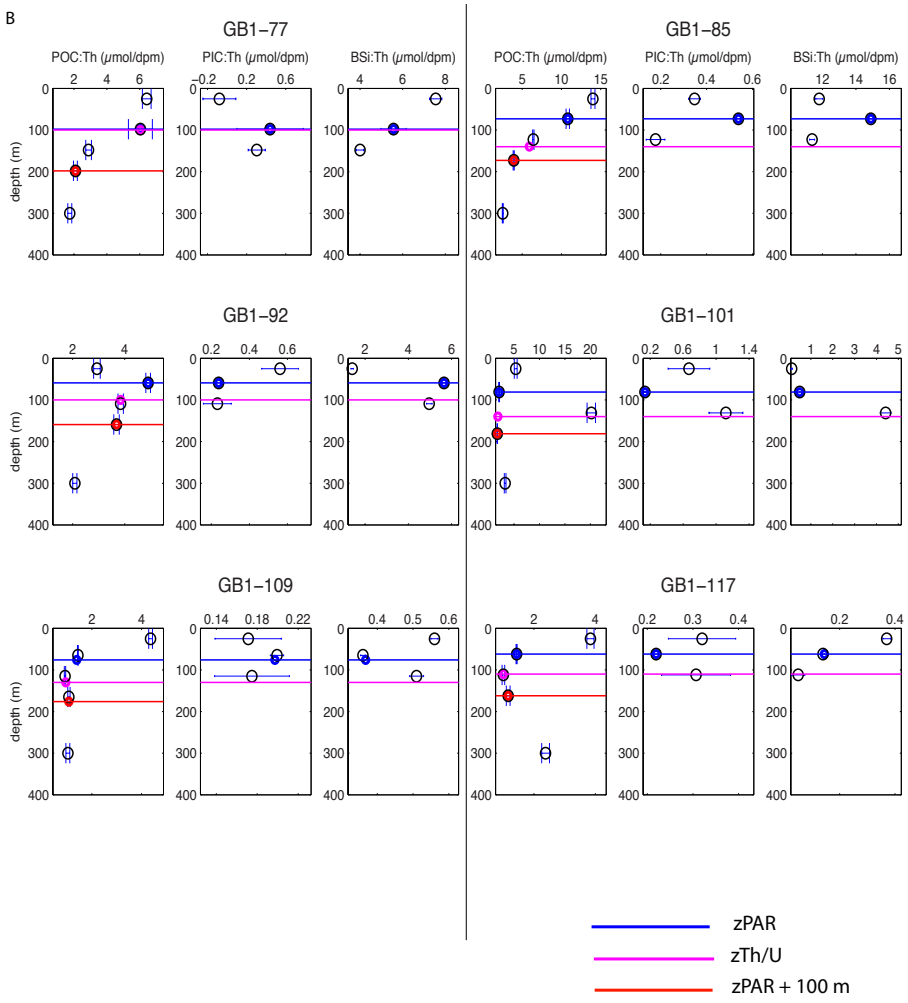
B
GB1–77
GB1–85
GB1–92
GB1–101
GB1–109
GB1–117
POC:Th (μmol/dpm)
PIC:Th (μmol/dpm)
BSi:Th (μmol/dpm)
depth (m)
zPAR
zTh/U
zPAR + 100 m

C

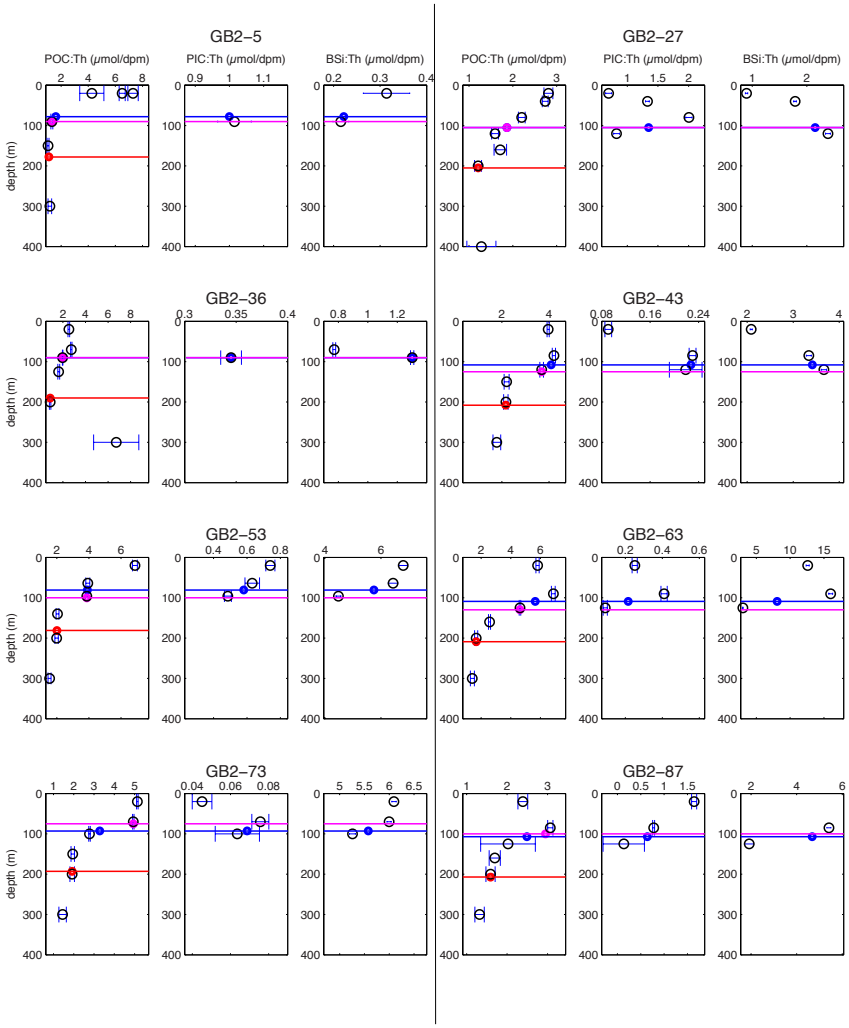
GB2–5
POC:Th (μmol/dpm)
PIC:Th (μmol/dpm)
BSi:Th (μmol/dpm)
GB2–27
GB2–36
GB2–43
GB2–53
GB2–63
GB2–73
GB2–87
depth (m)

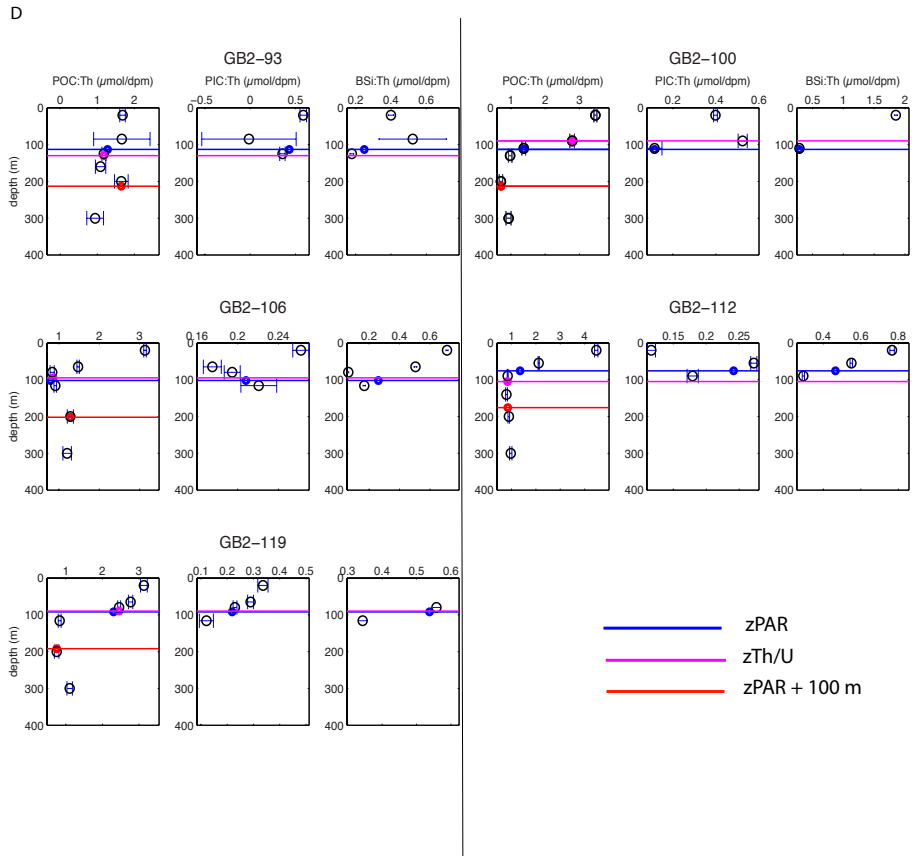

Figure S1. Profiles of >51 μm POC:^{234}Th, PIC:^{234}Th and BSi:^{234}Th above 400 m. Black open circles represent measurements. Colored circles represent values at three possible depths (colored lines; see legend) in the POC:^{234}Th panels, and at z_{PAR} (blue line) for the PIC:^{234}Th and BSi:^{234}Th panels. These values were interpolated when there were no measurements at these depths (refer to Tables 2 and 3 for specific stations). At station GB2-106, the BSi:^{234}Th interpolation calculation excluded the anomalously low value at 80 m. Error bars shown are the propagated errors of >51 μm [POC], [PIC], [BSi] and particulate ^{234}Th activity measurements. Note that "negative" values are below the instrument detection limit (see Sect. 2.3), and are equal to 0 within error.

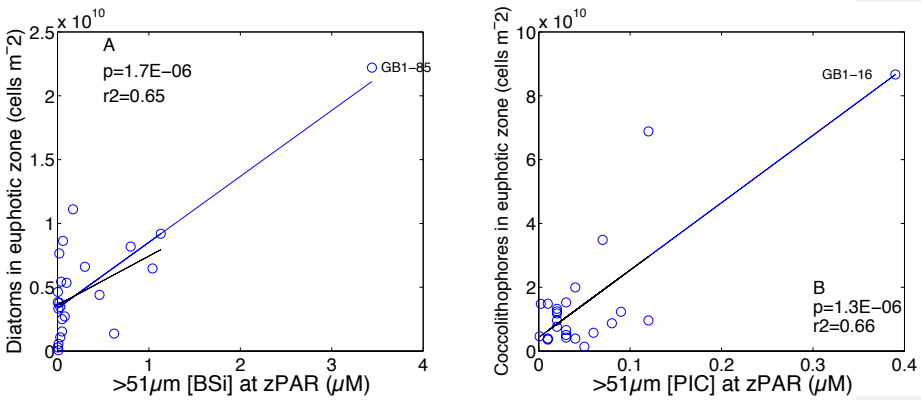

Figure S2. (A) Diatom cell counts integrated from surface to z_{PAR} (cells m^{-2}) as a function of >51 µm [BSi] at z_{PAR}. (B) Integrated coccolithophore cell counts as a function of >51 µm [PIC] at z_{PAR}. Outliers for >51 µm [BSi] and [PIC] at stations GB1-85 and GB1-16, respectively, are defined according to Chauvenet's Theorem (Glover et al., 2011). Total euphotic zone cell counts of diatoms and coccolithphores are significantly correlated to >51 µm [BSi] and [PIC] at z_{PAR} , respectively. The significant linear relationships are plotted here as blue lines, with corresponding p and r^2 values indicated. The regressions remain significant ($p<0.05$) even when excluding the outliers GB1-85 (Fig. S2a) and GB1-16 (Fig. S2b) from analysis (black lines). We note that cell counts are only available for the <36 µm size-fraction because of the methodology used for enumeration (see Supplemental Methods), while the biomineral measurements are of the >51 µm particle size-fraction (Sect. 2.2). Nonetheless, these relationships suggest that the >51 µm [BSi] and [PIC] at z_{PAR} do scale with the abundance of diatoms and coccolithophores in the euphotic zone of the water column.

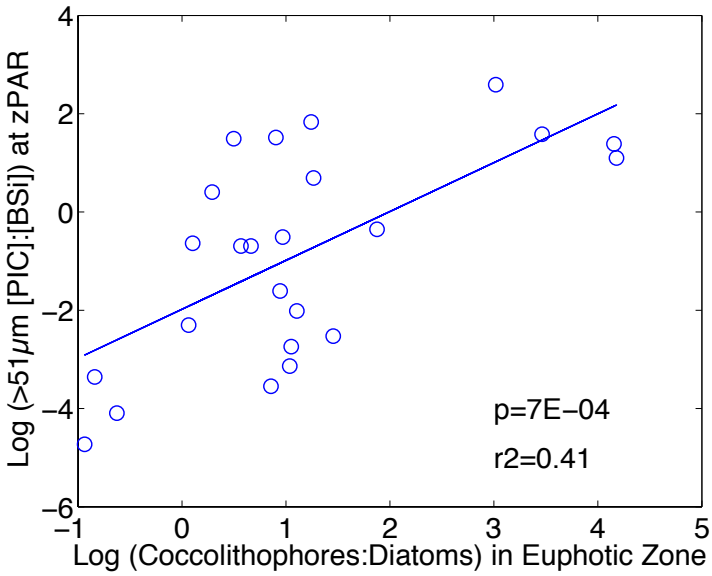

Figure S3. The natural log of the ratio of >51 μm [PIC]:[BSi] at z_{PAR} as a function of the natural log of the ratio of integrated coccolithophore: diatom cell counts in the euphotic zone. The significant linear relationship is plotted as a blue line, with a corresponding p and r^2 value indicated. This further supports the application of >51 μm size-fraction biomineral concentrations at z_{PAR} as a proxy for describing euphotic zone ecosystem composition in Sect. 4.7 and Fig. 10. Despite the different size-fractions that are represented by the biomineral measurements and the cell counts (see Supplemental Methods), the significant correlation nonetheless supports the use of >51 μm biomineral concentration ratios to describe the proportional abundance of certain phytoplankton types.

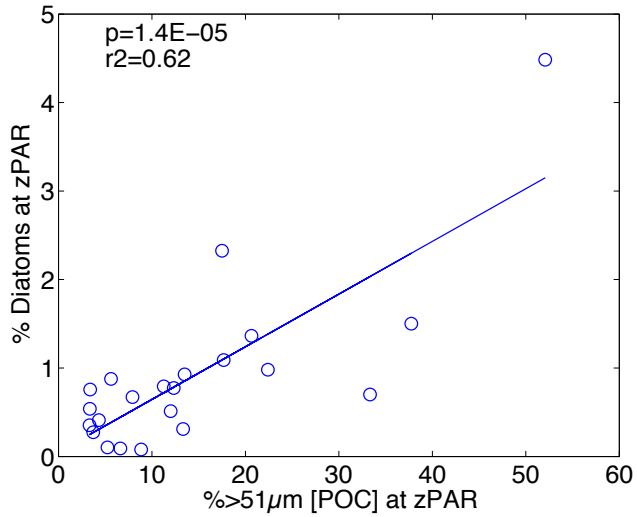

Figure S4. Percentage of total cells that are diatoms at z_{PAR} as a function of the % >51 µm [POC] at z_{PAR}. The significant linear relationship is plotted as a blue line, with a corresponding p and r^2 value indicated. This relationship shows that FlowCAM® measurements of diatom abundance support our interpretation that the size fractionation of POC (% >51 µm [POC] at z_{PAR}) determined from in-situ pump particle measurements (Sect. 2.2) reflects the relative abundance of diatoms. We note that there is no significant relationship between relative coccolithophore abundance and the size fractionation of POC.

Supplementary Methods for Figs. S2-S4

The FlowCAM® imaging cytometer enumerated nano- and microplankton cells from 10 mL Niskin cast samples at all McLane pump stations except GB2-36, GB2-27 and GB2-119 (refer to Table 1 for station locations) (Poulton and Martin, 2010). Moreover, at stations GB1-38 and GB1-70, cell counts were missing at z_{PAR}, and only measured at depths above and below z_{PAR}. The size range of counts was 5.6-35.5 µm. While particles >36 µm (up to 200 µm) could be seen in the FlowCAM®, they were rare in 10 mL samples, such that their normalized abundance could not be accurately calculated. Total diatom cell counts in the euphotic zone were approximated by summing FlowCam® -derived diatom concentrations (cells/mL) at all depths above z_{PAR}:

$$\text{total cell counts} = \sum_{1}^{\text{end}} \text{mean}\left[\frac{\text{cells}}{\text{mL}}_{n}, \frac{\text{cells}}{\text{mL}}_{n-1}\right] \times [z_n - z_{n-1}]$$

where n is the measurement index number from the surface depth at n=1 downward towards z_{PAR} at n="end". The unit for this summation is equivalent to cells m^{-2}. Coccoliths and plated cells in the same Niskin samples were counted by birefringence microscopy (Balch et al., 2011). Total coccolithophore counts in the euphotic zone (cells m^{-2}) were similarly estimated by summing the microscopy-based concentrations at all depths above z_{PAR}.

Supplementary References

Balch, W. M., Drapeau, D. T., Bowler, B. C., Lyczskowski, E., Booth, E. S., and Alley, D.: The contribution of coccolithophores to the optical and inorganic carbon budgets during the Southern Ocean Gas Exchange Experiment: New evidence in support of the Great Calcite Belt hypothesis, J. Geophys. Res., 116, C00F06, 2011.

Glover, D. M., Jenkins, W. J., and Doney, S. C.: Modeling methods for marine science., Cambridge University Press, 2011.

Poulton, N. J., and Martin, J. L. Imaging flow cytometry for quantitative phytoplankton analysis - FlowCAM. In: Karlson B, Cusack C, Bresnan E (eds) Microscopic and molecular methods for quantitative phytoplankton analysis, Vol Chapter 8. Intergovernmental Oceanographic Commission of UNESCO, Paris, France, 49-54, 2010.